N66-15632

Semi-Annual Status Report

for the period March 1, 1965 to August 31, 1965

NASA Grant NsG-655/36-013-002

Principal Investigator: Karl J. Casper

Summary

The research covered by this status report can be divided into the following topics:

(1) Studies of the fundamental response of semiconductor detectors to charged particles.

(2) Fabrication techniques for lithium surface barrier silicon detectors.

(3) Compilation of the computer program for the analysis of beta decay spectra.

(4) Operation of a superconducting magnet in conjuction with solid state detectors as a novel and unique beta ray spectrometer.

(5) Direct observation of the internal Compton effect with the superconducting magnet beta ray spectrometer.

(6) Studies of high Z semiconductors for improved gamma ray detection.

(1) It was proposed to study the response of silicon detectors to electrons of different energies. This is most important from the standpoint of analysis of beta ray spectra since the response function has been found to vary from detector to detector. Silicon detectors with different configurations, resistivities, dislocation densities, and orientations will be used in order to determine the dependence of the response function on these characteristics. For this purpose a commercial electromagnet has been purchased and is scheduled for delivery by September 1, 1965. A simple beta ray spectrometer is being constructed and will be used for these studies. An exotic instrument is not necessary since the solid state detector itself will be used for the energy calibration. The only requirement is that the spectrometer produce a beam of electrons with a relatively narrow energy spread. These experiments will be reported in the annual report.

A vacuum system with a larger diffusion furnace has been completed for the diffusion of large volume silicon and germanium detectors. The original furnace used for this purpose proved to be too small and produced an excessive amount of side diffusion of lithium and an uneven junction in these large crystals. In processing the crystal, it was necessary to reduce the crystal size excessively, and even then the reverse current was too large by an order of magnitude for effective lithium ion drifting. We expect that this problem will be corrected with the new furnace.

Large silicon detectors have high capacitances as a result of their large areas. Moreover, the surface currents are relatively high since high voltages must be used and since the exposed junction surface is quite

large. An attempt was made to reduce both of these factors by drifing a silicon detector in such a way that the p contact area was substantially reduced. Lithium was diffused into the sides and one surface of the crystal. The other contact was made in the center of the other surface, and the crystal was drifted in FC-43 fluorochemical. In Fig. 1, the crystal is shown during the actual drifting. The circle of bubbles on the surface indicates the junction region. The drift is proceeding toward the center of the crystal.

Fig. 2 shows the crystal in cross section after drifting, and after stain etching. The p-type material which is uncompensated is stained very dark, the n-type lithium rich region is stained very light, and the lithium-ion compensated region is intermediate in tone. From this figure it can be seen that the area of contact between the p layer and the intrinsic region is quite small. Ordinarily, the entire top surface would constitute the p-type region.

After the drift, it was found that the reverse current leakage was about the same as most detectors at room temperature. It has been our experience in the past with junctions formed on the [111] surface that the currents are rather high. In this case only a small reduction, perhaps a factor of two, could have been expected. Hence, the measurement of the reverse current which depends on a number of things is not too significant. When cooled to liquid nitrogen temperature, however, the current was reduced below 10^{-7} amps and the detector operated very successfully. Moreover, and more significantly, the capacitance of the detector was only 15 pf at liquid nitrogen temperature. Detectors of this size ordinarily have capacitances greater than 50 pf. Since the noise is directly related to the detector

Fig. 1 Large volume detector during drift in FC-43 fluorocarbon. The bubbles indicate the drifted region.

Fig. 2 Cross-section of large volume detector after drifting and stain etching.

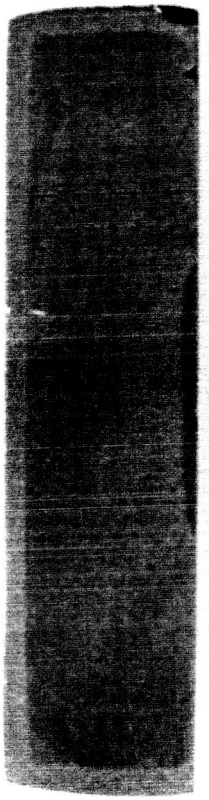

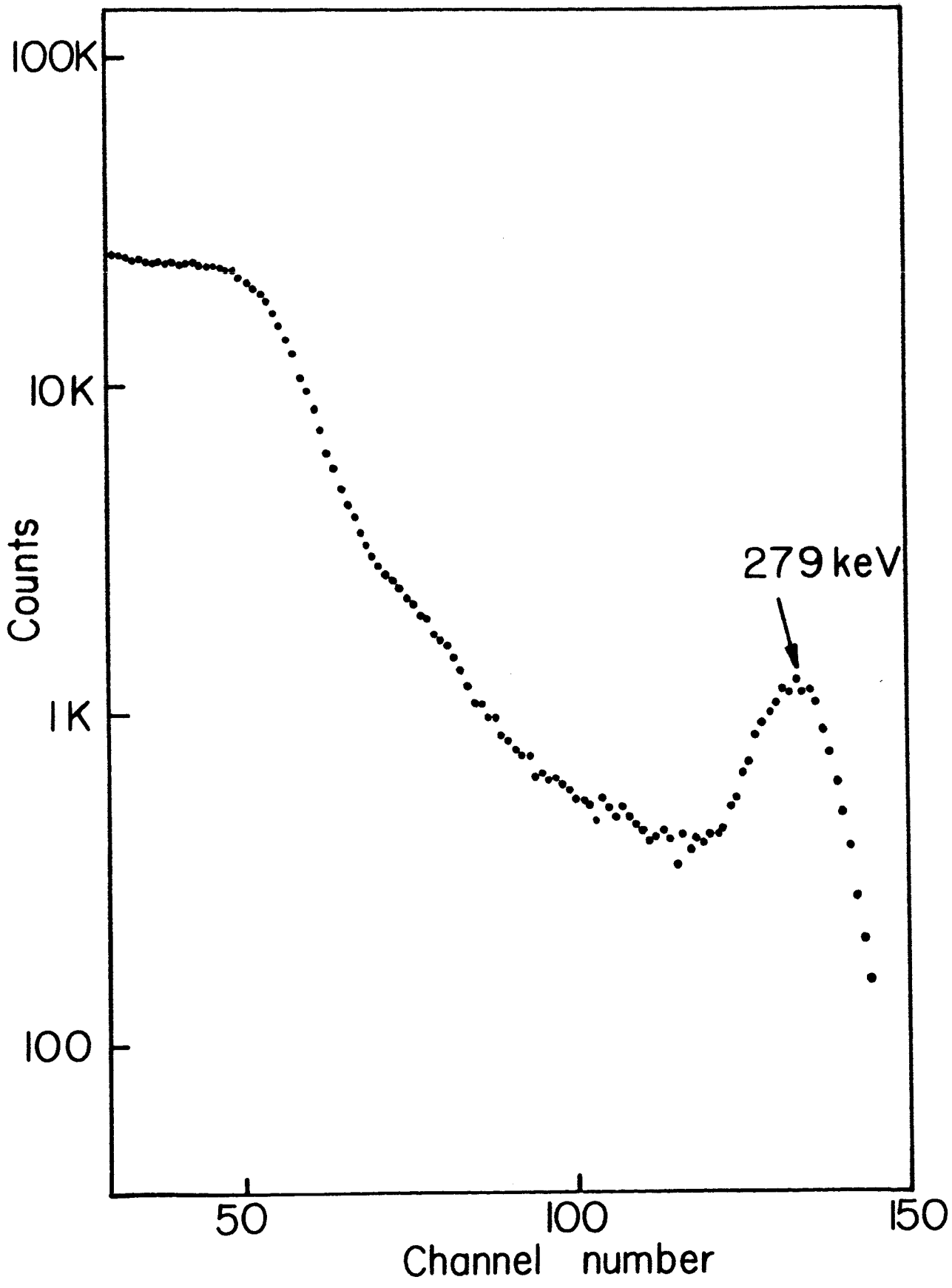
100K
10K
1K
100
Counts
279 keV
50
100
150
Channel number

capacitance, such detectors should have inherently lower noise and therefore better resolutions than detectors of the same size but with ordinary configurations. One disadvantage of this detector can be seen in Fig. 2. There is still a small window of original p-type material which can interfere with measurements of heavy charge particles and would therefore have to be masked off from the incident beam.

The low Z of silicon makes it difficult to use for gamma-ray detection although the large volume of this detector somewhat compensates for it. Two spectra are shown in Figs. 3 and 4, illustrating the detection capabilities for gamma rays of Hg^{203} and Cs^{137}. It is apparent that the Compton effect whose cross section is high relative to that for the photoelectric effect at these energies would mask many gamma ray transitions in a decay where a large number of gamma rays appear.

There have been a number of recent papers describing experiments[2-7] with accelerators which demonstrate the importance of crystal orientation on the charged particle energy loss. Essentially, it has been shown that if the crystal is oriented so that the charged particle beam is incident along the [111] or [110] axis, the energy loss per unit of range may be considerably lower than the average expected loss. As a result of glancing atomic collisions, the ions are channeled along particular directions in which the electron density is relatively low. Since most of the energy loss occurs through collisions with electrons, the range of the particle in silicon may be significantly increased. Spectral distortion and incomplete energy loss in a particular detector may be the result.

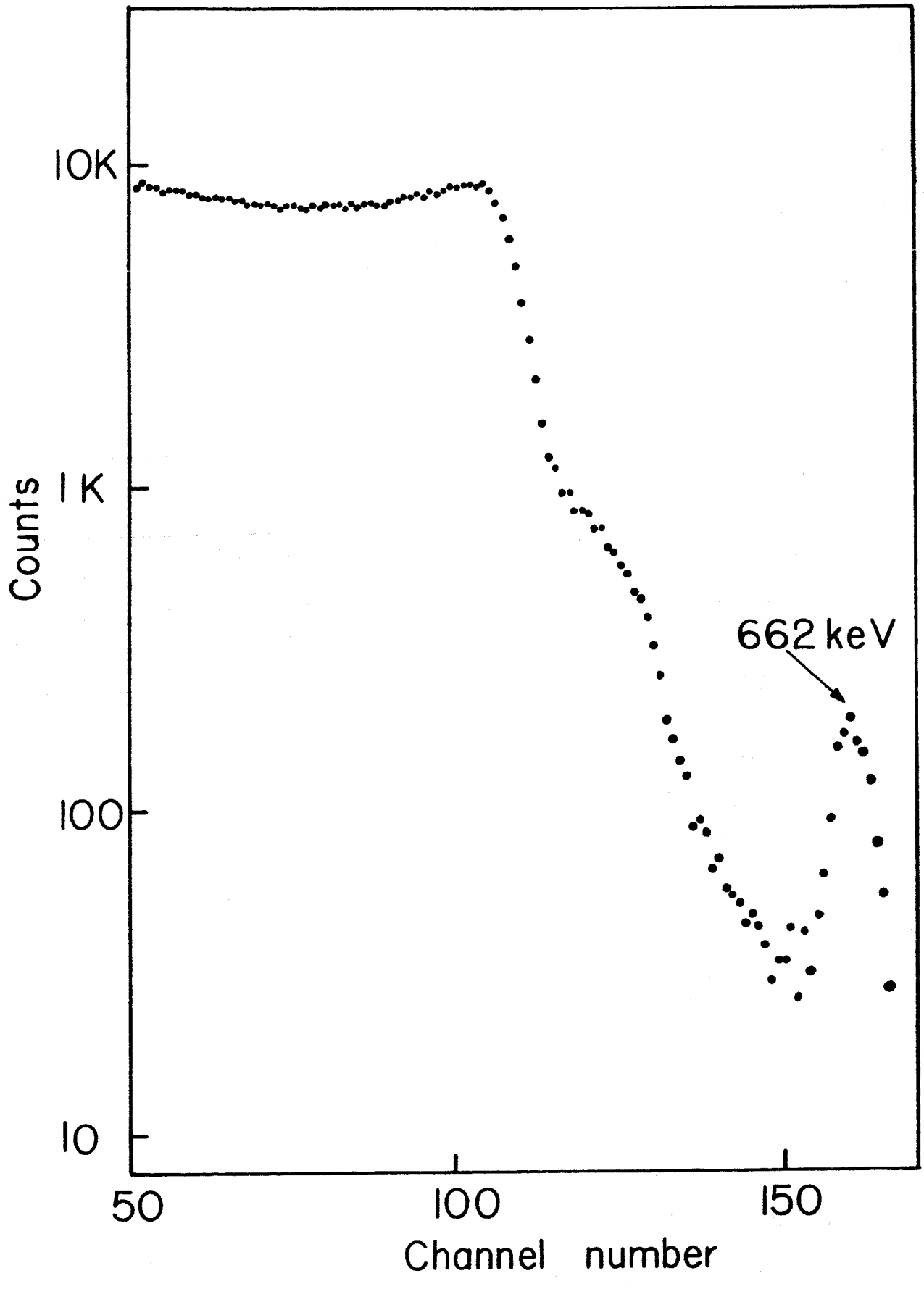
10K
1K
100
10
Counts
662 keV
50
100
150
Channel number

Fig. 4 Gamma ray spectrum of Cs^{137} as measured with the large volume detector of Fig. 2.

Two sets of silicon wafers cut from the same ingot have been obtained from Geoscience Instruments Corporation. The first set is sliced perpendicular to the [111] axis and, when these are fabricated as detectors, should exhibit this anomalously lower energy loss. The second set of slices were cut approximately 20^0 from the [100] axis in the direction of the [110] axis and 8^0 off the [110] axis in the direction of the [111] axis. One of these slices is shown in Fig. 5. It has been suggested[3] that for particles incident on a detector made from this crystal, the energy loss will be maximized and will be very close to the average energy loss expected. These detectors are now being finished and will be tested to determine if there are any substantive differences in the measured spectra.

Finally, copper plating techniques have been used in the past on germanium to reduce the precipitation of lithium. The copper is plated prior to any processing and diffused into the germanium on a hot plate. We have found that drifting large volume detectors by this method was rather difficult. The lithium drift tended to stop at about 5 to 6 mm, and, in some cases, it was impossible to drift at all. We have altered this technique in the following manner. Copper is plated onto the germanium crystal in the usual manner, but not diffused. Lithium is then evaporated onto one surface, and both the lithium and the copper are diffused at the same time at 370^0 C. The wafer is then removed from the system and cooled to liguid nitrogen temperature. At this temperature, the lithium is nearly immobile, but the copper is still mobile and over a period of several days will diffuse throughout the crystal filling us the vacancies. We have

Fig. 5 Silicon crystal cut 20^0 from [100] axis in direction of the [110] axis and 8^0 off the [110] axis in the direction of the [111] axis.

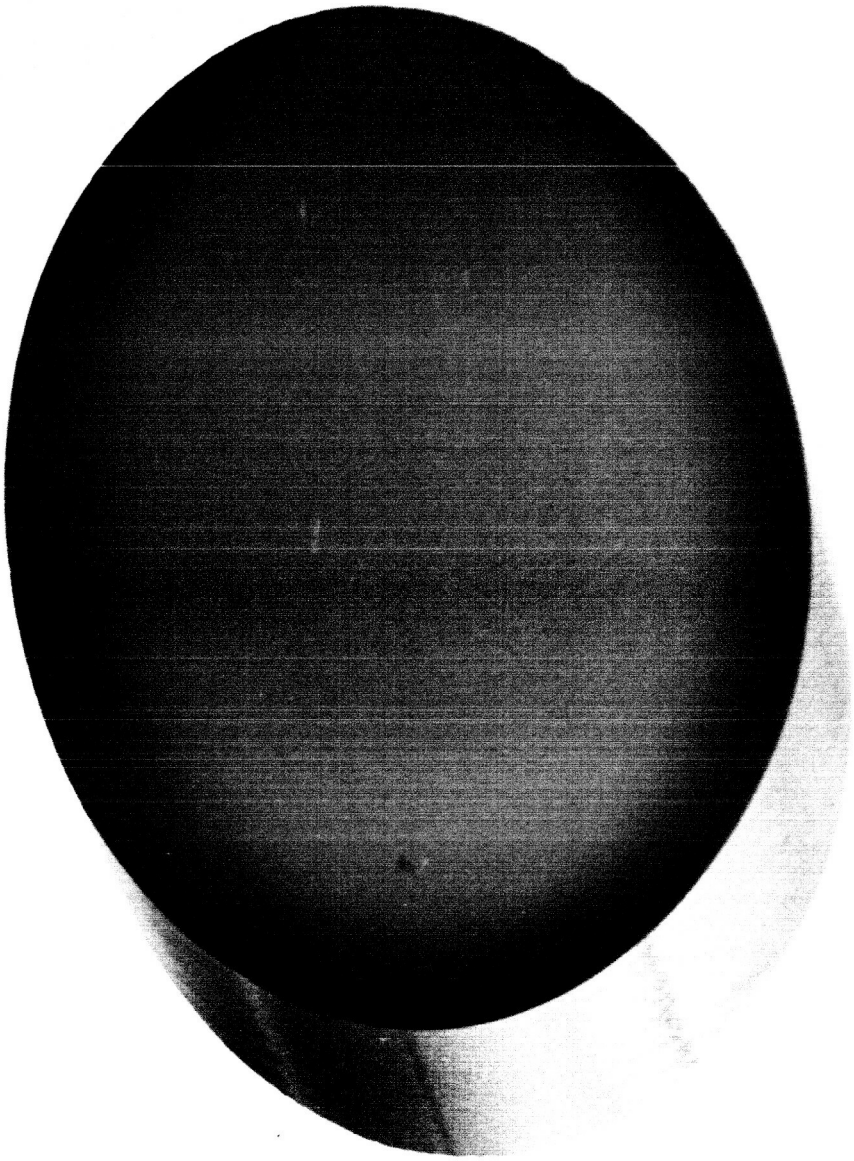

found that it has been possible to drift nearly to the back of the crystal after this treatment. In some of the crystals in which no drift had been possible before, lithium-ion drifting occurred quite readily.

(3) Fabrication techniques for lithium drifted silicon surface barrier detectors. This section is being submitted for publication to Nuclear Instruments and Methods. A preprint is attached to this report.

(3) Compilation of the computer program for the analysis of beta ray spectra measured by lithium drifted surface barrier silicon detectors. We have received several inquiries about the program used in the paper "Beta Decay of Rb^{86}", a preprint of which was attached to the annual report for the period March 1, 1964 to February 28, 1965. As a result the program has been compiled and a complete description of the steps prepared. This is being submitted to the Subcommittee for Nuclear Structure of the Committee on Physical Sciences of the National Research Council, National Academy of Science for inclusion in their list entitled Abstracts of Computer Codes. A copy is attached to this report.

(4) We have performed recent experiments using silicon solid state detectors in conjunction with a superconducting solenoid as a novel form of beta ray spectrometer. Although this work was begun a couple of years ago, it was able to be continued only by virtue of this grant. A diagram of the apparatus is shown in Fig. 6. The two detectors are mounted at the ends of a probe with a radioactive source in the center, and this probe is then placed in the superconducting solenoid. At fields of 25 to 30 kilogauss, all of the beta rays emitted by the source are confined to a cylinder of 2 to 4 mm radius along the axis of the spectrometer. In this

Fig. 6 Superconducting magnet beta ray spectrometer.

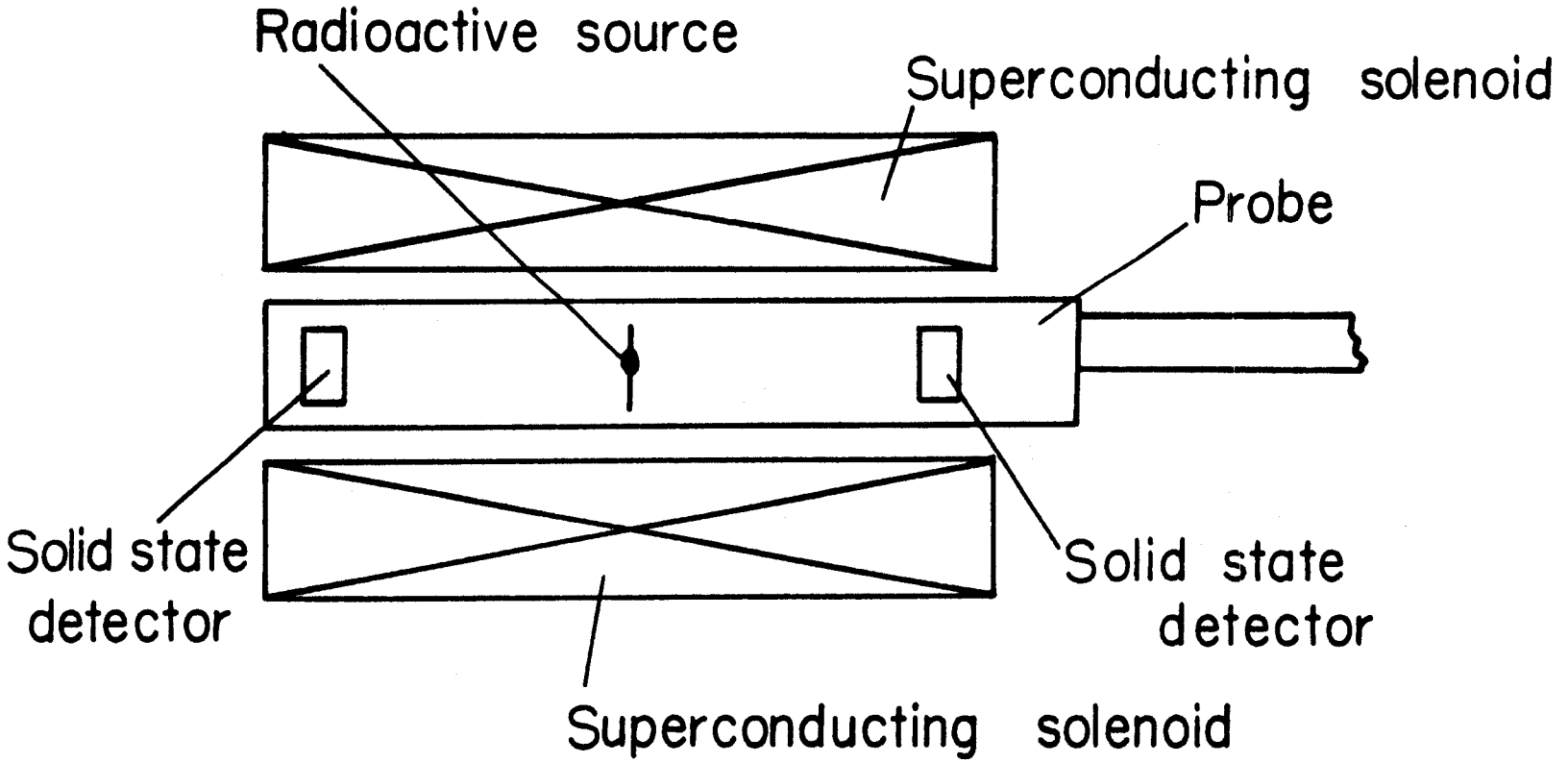
Radioactive source
Superconducting solenoid
Probe
Solid state detector
Solid state detector
Superconducting solenoid

way they must be incident on one of the two detectors. A true 4π beta ray spectrometer is obtained with many advantages over conventional spectrometers: (1) The absence of any baffles for focussing electrons elininates one of the primary causes of spectral distortion. (2) The 4π geometry enables one to use very weak sources, on the order of 20 nanocuries. This means that the source thickness and hence the electron scattering in the source is considerably reduced which eliminates much of the spectral distortion at low energies produced by this effect. (3) Since solid state detectors are used, no energy selection by the magnetic field is necessary since the detectors themselves determine the energy of the beta ray. It is therefore unnecessary to take point by point plots such as is done with conventional spectrometers, since all counts are recorded with a multichannel analyzer. (4) Finally, the gamma ray flux striking the detector is reduced by the solid angle since there is no focussing of the gamma rays by the magnetic field. This reduction is shown in the comparison of the two Bi^{207} spectra in Fig. 7. The Compton distribution has been significantly reduced by the use of the spectrometer.

The initial experiments have used only one detector at a time. The increase in collection is in good agreement with source strength determined from knowing the specific activity and the amount of material pipetted onto the source backing. However, in Fig. 7, it is readily seen that the backscattering tail is still a significant fraction of the spectrum.

Recently, experiments have been performed in an effort to elimintate this tail. The two detectors mounted in the probe were run in parallel

Fig. 7 Comparison of Bi^{207} spectrum measured in superconducting solenoid to spectrum measured outside solenoid with source close to detector showing diminution of gamma-ray background.

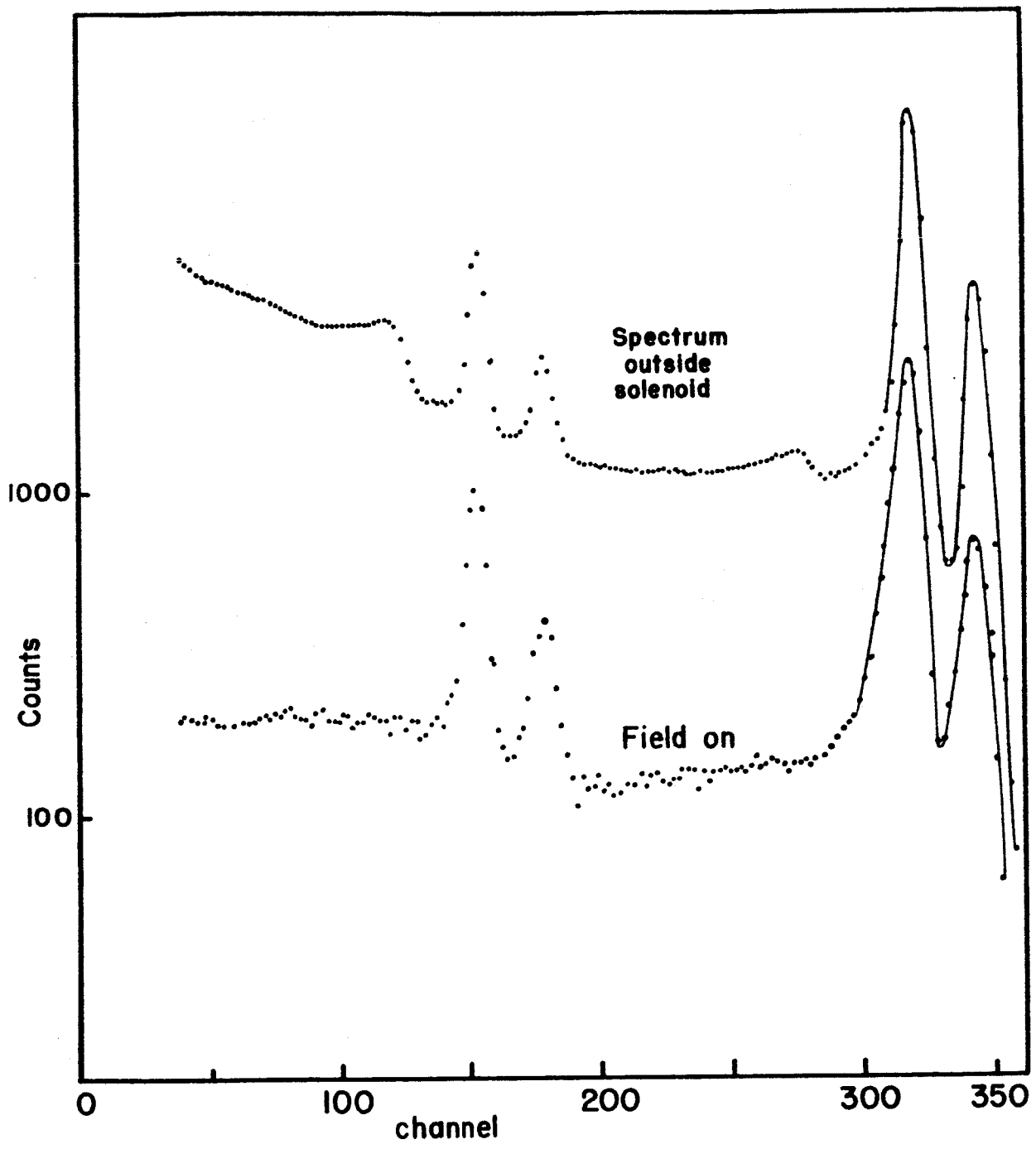
Spectrum
outside
solenoid
Field on
1000
100
Counts
0
100
200
300
350
channel

from the same preamplifier. Electrons backscattered from one detector are still confined to move in the axial cylinder and will be incident on the detector at the other end of the probe. Thus, in this coincidence arrangement, the total electron charge should be collected and the backscattering tail eliminated. The Bi^{207} spectrum measured in this way is shown in Fig. 8. The backscattering has been eliminated, but a new tail much smaller in amplitude is evident. Some continuous beta-ray spectra were also measured, and this data is now being analyzed to determine if these spectra are undistorted. As soon as that analysis is complete, a paper on the operation of the spectrometer will be submitted to the Review of Scientific Instruments.

(5) As mentioned in Section 4, a different type of tail can be seen when the detectors are operated in parallel. This tail appears to consist of electrons produced by the internal Compton effect.[8] The measurement here, insofar as we can determine, is the first direct spectral observation of this effect.

The internal Compton effect is a quantum mechanical process quite analogous in the classical limit to internal bremsstrahlung. The internal conversion process consists of the emission of an orbital electron instead of a nuclear gamma ray with energy equal to the transition energy less the binding energy of the electron. Accompanying this process is a continuous gamma ray spectrum and a continous electron spectrum which is the result of the scattering of an outgoing photon from one of the orbital electrons with the possible emission of the electron. In the ordinary Compton effect, the nucleus does not participate in the scattering process and the electron

Fig. 8 Bi^{207} spectrum measured with the two detectors in the spectrometer run in coincidence in order to remove the backscattering tail.

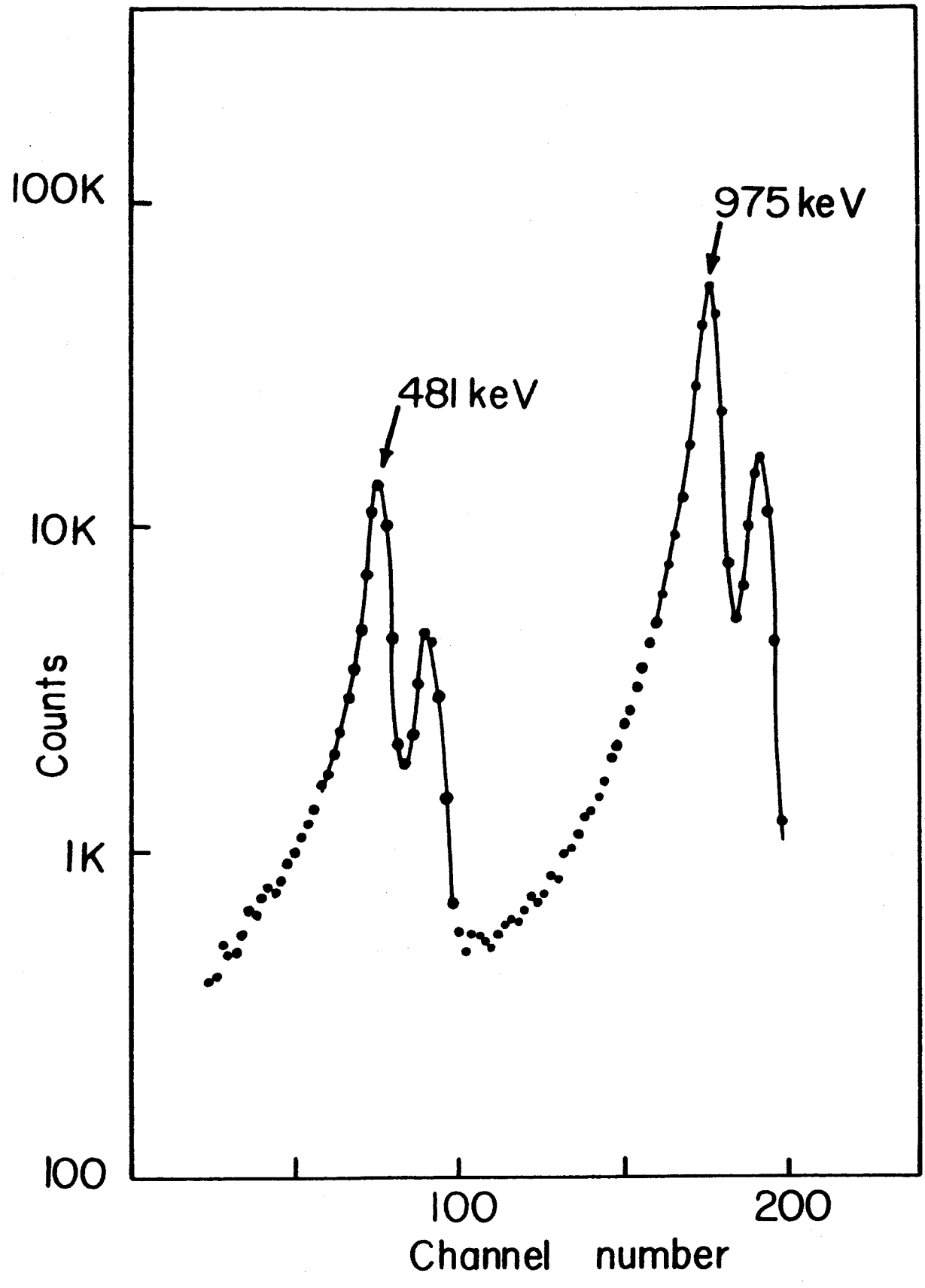
100K
10K
1K
100
Counts
481 keV
975 keV
100
200
Channel number

has a maximum energy given in the case where the gamma ray strikes the electron and recoils at an angle of 180^0. In the internal Compton effect, however, the nucleus is available to participate in the momentum exchange and therefore no Compton edge is observed.

Calculations of the internal Compton effect have been made by Cooper and Morrison,[9] Spruch and Goertzel,[10] and two Russians.[11,12] Cooper and Morrison limited themselves to high-energy electric dipole transitions, Spruch and Goertzel to magnetic multipole transitions, and the Russians to electric multipole transitions, but with a Z = 0 approximation which means that these results are of little practical use. To date no calculations exist for electric multipole transitions taking into account the Z of the nucleus. As a result, it is difficult to interpret most experimental results.

Fortunately, the 1063.4 keV transition in Bi^{207} is a pure M4 transition. The formulas of Spruch and Goertzel are therefore applicable. From the intensity of the 975 keV K internal conversion line and the measured value of the internal conversion coefficient, the absolute strength of the source can be calculated thereby determining the intensity of the internal Compton effect. The theoretical expression was integrated over all angles, the distribution was corrected for the finite energy resolution of the detectors, and both the K and L conversion line contributions were taken into account. The comparison between theory and experiment is shown in Figs. 9 and 10. The agreement is remarkable considering the approximations that are used for the theoretical calculations. The theory is severely tested for low

Fig. 9 This is an enlarged portion of Fig. 8 showing the 975 keV internal conversion line with the remaining tail. The circled dots are the data points, the x's are the calculated points for the internal Compton effect with binding energy included, and the triangular points are the calculated points for the internal Compton effect not including the binding energy in the calculations.

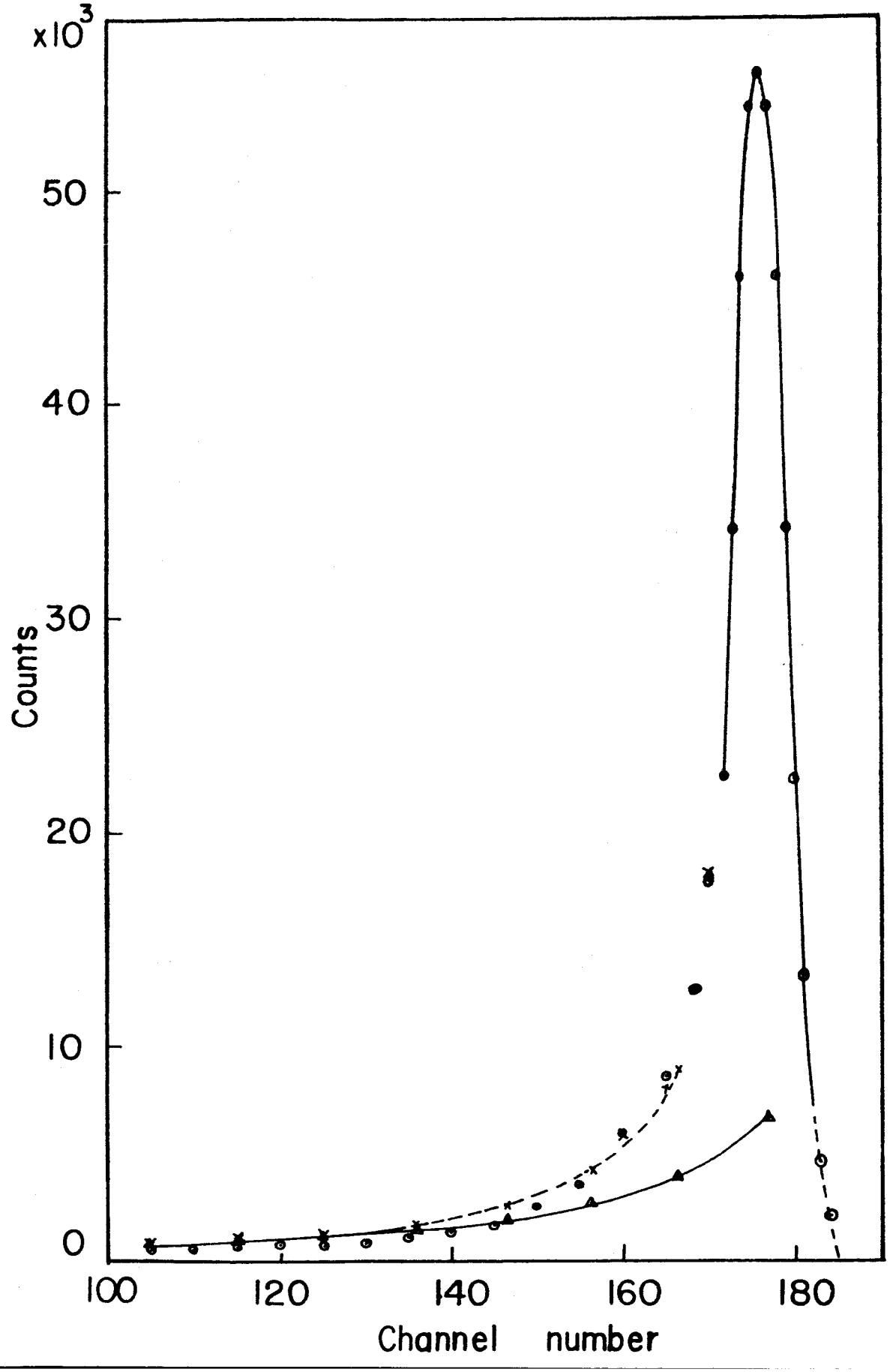
x10^3
50
40
30
20
10
0
Counts
100
120
140
160
180
Channel number

Fig. 10 This is the same comparison as Fig. 9, except plotted on semi-logarithmic paper. The triangular dots are the calculated points with binding energy considered, the circled dots are the calculated points with no binding energy included, and the small dots are the data points.

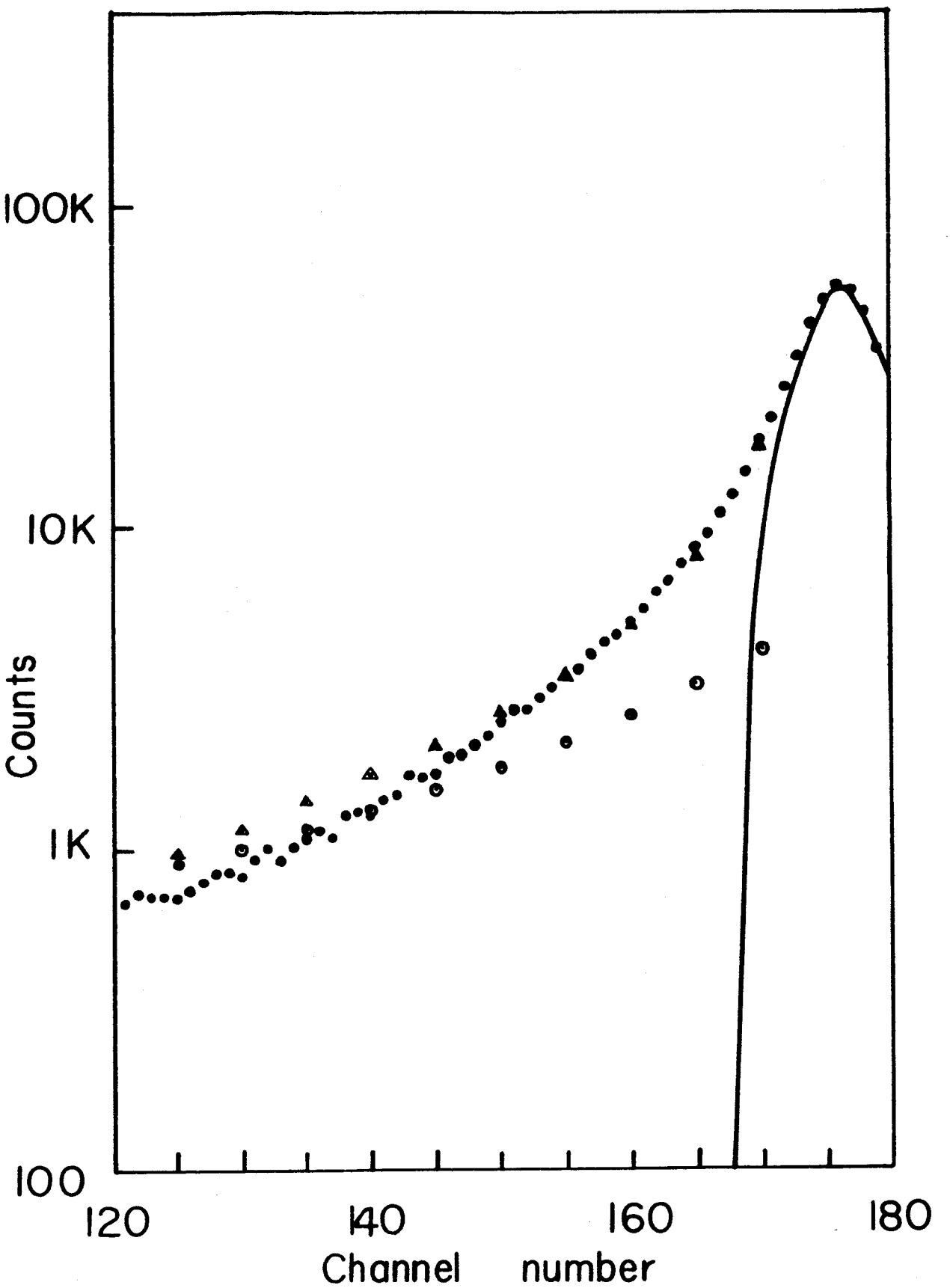
100K
10K
1K
100
Counts
120
140
160
180
Channel number

gamma ray energies, that is, for electron energies near the internal conversion peak itself. This is evident from the increasing disagreement as the conversion line energy is approached.

Some previous experimental measurements have been made by Brown and Stump[13] and by Lindqvist, Pettersson and Siegbahn[14] on the nucleus Cs^{137}. The measurement performed by them is much more difficult since the continuous beta ray spectrum from the natural beta decay has an end-point energy near the conversion line. In both cases, angular correlations between the gamma rays and the scattered electrons were measured with no agreement in one experiment and only rough agreement in the other.

Thus, the experiment performed with the superconducting solenoid appears to be the first direct spectral observation of this effect. Because of the extremely small source strength (about 5 orders of magnitude smaller than that used in conventional spectrometers) and because of the configuration of the spectrometer, we feel that this effect is certainly not ascribable to any instrumental effect as is the case with convential spectrometers. These results on the internal Compton effect indicate that the spectrometer itself is a sensitive instrument subject to little distortion, and capable of the most refined measurements.

(6) The first high Z semiconductor to be studied has been indium antimonide. Doped samples with high resistivities ($\sim$ 30 ohm-cm) were obtained from Monsanto. The chemical processing and etching techniques used were similar to those for germanium and silicon and good polish etches could be obtained. Unfortunately, the doped carrier concentrations were

substantially below the intrinsic carrier concentration. As a result, the crystal was n-type at room temperature, changing to p-type near liquid nitrogen temperatures. Lithium diffusions could be made into the material itself, but the diode structure was not stable and even at liquid nitrogen temperature, the reverse current was very high. Additional crystals will be obtained, but the problem is to find crystals in which the carrier concentration of the impurity is higher than the intrinsic carrier concentration, yet lower than the diffused lithium concentration.

Gallium antimonide crystals have been on order with several suppliers for more than three months, but these suppliers are apparently having difficulty growing this material to specification. We have been in contact with Dr F. J. Reid of Batelle Memorial Institute, who has some gallium antimonide crystals with low carrier concentrations which were especially grown for him. He has promised to send us some of these in the near future.

REFERENCES

1. J. L. Blankenship, JEEE Trans. on Nucl. Sci. NS-11, No. 3 (1964) 373.
2. G. Dearnaley, IEEE Trans. on Nucl. Sci. NS-11, No. 3 (1964) 249.
3. H. E. Wegner and C. Erginsoy, IEEE Trans. on Nucl. Sci. NS-12, No. 1 (1965) 240.
4. C. D. Moak, Bull. Am. Phys. Soc. 10 (1965) 515.
5. W. W. Walker, C. D. Moak, and J. W. T. Dabbs, Bull. Am. Phys. Soc. 10 (1965) 515.
6. G. Dearnaley and A. R. Sattler, Bull. Am. Phys. Soc. 10 (1965) 515.
7. A. R. Sattler and G. Dearnaley, Bull. Am. Phys. Soc. 10 (1965) 515.
8. See, for example, B.-G. Pettersson, The Internal Compton Effect in Alpha- , Beta- and Gamma-Ray Spectroscopy (ed. K. Siegbahn, North-Holland Publishing Co., Amsterdam, 1964) 1579.
9. E. P. Cooper and P. Morrison, Phys. Rev. 57 (1940) 862.
10. L. Spruch and G. Goertzel, Phys. Rev. 94 (1954) 1671.
11. E. G. Melikian, JETP 4 (1957) 930.
12. A. M. Iakobson, JETP 2 (1956) 751.
13. H. B. Brown and R. Stump, Phys. Rev. 90 (1953) 1061.
14. T. Lindqvist, B.-G. Pettersson, and K. Seigbahn, Nucl. Phys. 5 (1958) 47.

N66-15633

Fabrication Methods for Lithium Drifted Surface Barrier Silicon Detectors*

H. M. Murray, J. W. Harpster† and K. J. Casper

Department of Physics, Western Reserve University, Cleveland, Ohio

Techniques for the fabrication of lithium surface barrier silicon detectors are presented. All important chemical procedures are described in detail. The detectors made by these techniques exhibit resolutions of 15 to 30 keV on internal conversion electrons when operated at room temperature.

1. Introduction

A number of papers[1-7] have appeared describing methods of fabricating lithium drifted solid state silicon detectors. The detectors described in these papers either have not been of the surface-barrier type or else require cooling for best operation. The methods described here are consistently dependable for the preparation of surface barrier types which exhibit good resolution at room temperature.

2. Chemical Specifications

Electronic grade chemicals are used throughout the fabrication process. Either absolute ethanol or methanol is suitable where the use of alcohol is specified. The acid concentrations are 70% HNO_3, 48% HF, and glacial

*Supported in part by a grant from the National Aeronautics and Space Administration.

†Present address: Department of Electrical Engineering, Ohio State University, Columbus, Ohio.

acetic acid, and all etches are prepared and used in a Teflon beaker. Baker Atomex Immersion Gold Solution* is used in the electroless gold plating. The lithium is obtained in the form of rods† and is kept stored in mineral oil. For evaporation, the desired amount of lithium is cut off the end of the rod with a diagonal wire cutter and cleaned with trichloroethylene. Vinyl gloves†† are worn whenever the crystal must be handled, and the etched sides of the crystal are kept scrupulously clean. Generally, stainless steel tweezers are used to hold the crystal wherever possible.

In discussing the crystal after lithium diffusion, the term "front surface" refers to the surface on which lithium has been diffused, and "back surface" refers to the surface toward which the lithium is drifted.

3. Crystal Specification and Evaluation

The silicon crystals are obtained as wafers sliced and lapped to the desired thickness from Geoscience Instruments Corporation.* The silicon is specified to be p-type, boron doped, float-zone refined, 50-200 ohm cm, with a dislocation count less than 20,000/cm^2. The orientation is usually [111] although crystals cut with different orientations have been used.

As a first step the dislocation pattern is determined. A single slice from each ingot is etched in the following manner:

(1) The crystal is lapped first with 20 micron and then 10 micron

*Engelhard Industries, Inc., Baker Platinum Division, 113 Astor Street, Newark, N.J.

†Lithium Corporation of America, Bessemer City, North Carolina

††Wilson Tru-Touch, Becton, Dickinson and Co., Rutherford, New Jersey

*110 Beekman Street, New York, N.Y.

aluminum oxide powder, cleaned ultrasoncially in trichloroethylene, and washed successively in alcohol and distilled water.

(2) A 2:1 mixture of HNO_3 and HF is prepared in a Teflon beaker and cooled in ice water. The wafer is then etched for 45 seconds in this solution. The etch is quenched by placing the beaker under running distilled water until all of the etchant has been displaced by water. In all of the polish etches, no air is permitted to come into contact with the wafer while it is being activated by acids.

(3) The wafer is then placed immediately into a Teflon beaker containing a 10:3:1 mixture of HOAc, HNO_3 and HF in sufficient amount to immerse the wafer. The crystal is etched in this solution for at least four hours at room temperature, after which the etch is again quenched with distilled water.

In most of the crystals, an outer ring of high density dislocations is observed. Such a ring is evident in the crystal shown in Fig. 1. The size of this ring is approximately the same for all of the slices of the ingot. Therefore, before any further processing, this high dislocation ring must be removed from each crystal. If the dislocation density is high even in the center of the crystal, the ingot is rejected as unsuitable.

4. Preparation of the Crystal for Diffusion

Each crystal is sanded down to remove the high dislocation ring using the small lapidary wheel[†] shown in Fig. 2 and cloth backed, #320 silicon carbide discs. The crystal and the disc are kept moistened to prevent overheating of the crystal. The sides are then smoothed by

[†]Model NBMD, Lee Lapidaries, 6617 Lorain Ave., Cleveland, Ohio

light hand sanding with silicon carbide paper. The faces are lapped and the wafer is ultrasonically cleaned in trichloroethylene and washed successively with alcohol and distilled water.

5. Diffusion of Lithium

Two diffusion furnaces have been used. The first, shown in Fig. 3, is operated in a vacuum of about 10^{-5} mm. Lithium is evaporated from the basket onto the surface of the crystal. The furnace is then raised to a temperature of 370° C as measured with the platinum resistor.†† After five minutes, the current is turned off, and air is let into the system immediately. The crystal is then cooled by placing it on a carbon block. A crystal diffused in this manner is shown in Fig. 4. The dark lithium hydroxide circle indicates the area of diffusion. Diffusion of lithium on the sides of the crystal is minimized, but the final detector size is restricted by the aperture in the mounting plate.

The second furnace, shown in Fig. 5, is similar to the one used by Lothrop and Smith[7], and is also operated in a vacuum. Lithium metal is evaporated onto the surface of the unheated crystal. The crystal is then heated to a diffusion temperature of 370° C, as measured by mounting the platinum resistor on the heating plate. The valves for the pumps are closed, and approximately 1 liter of nitrogen gas is let into the bell jar. Under these conditions, the diffusion rate is 0.1 mm/minute for silicon, and a diffused layer of 0.1 mm for each mm of crystal thickness is used.

††C. E. #30707-7A, Engelhard Industries, Inc., Instruments and Systems Division, 850 Passaic Ave., East Newark, New Jersey

After diffusion, the current for the heating coil is turned off, air let into the vacuum system immediately, and the wafer cooled by placing it on a carbon block.

After the crystal has reached room temperature, the lithium hydroxide coating is washed from the surface of the silicon with distilled water. The face is lapped and the sides are sanded to remove all traces of this coating. The crystal is then scrubbed with cotton swabs moistened with distilled water.

6. Stain Etching

Stain etching techniques[8] are used to reveal the extent of the lithium diffusion. The stain etch is an accurate 1000:1 mixture of HF and HNO_3 in sufficient quantity that the wafer is completely covered by the solution in a small Teflon beaker. The beaker containing the wafer with the lithium diffused face down is placed directly under an incandescent light until hydrogen bubbles are seen on the sides and surface of the wafer. After the back surface has stained darkly, the wafer is removed from the etch and washed in distilled water. The p-type material should stain darkly in comparison to the n-type, lithium-rich region. The usual practice has been to ignore the results of the first etch of a freshly prepared solution and to lap and sand the crystal and etch it again in the same solution. Stain etch solutions can be used with satisfactory results for approximately an hour after mixing.

The crystal shown in Fig. 6 was diffused in the furnace of Fig. 5 and has been stain etched. This figure shows the importance of the stain etch

for determining the quality of the junction. Side diffusion of lithium has occurred on this crystal and must be removed before a good diode can be obtained. The crystal is sanded and checked with staining until the sides of the wafer show a sharp, even junction with no evidence of diffused lithium on the sides. Figure 7 shows the crystal of Fig. 6 after this processing.

With the crystal shown in Fig. 4, the sides are usually sanded down to the lithium hydroxide circle. At this point, the stain etch is used, and the crystal is sanded further, if necessary, until a good junction is observed.

7. Electroless Gold Contacting

The crystal is now lapped and sanded to remove the stain etch. As before, after sanding it is cleaned ultrasonically with trichloroethylene, rinsed successively with alcohol and distilled water, and scrubbed with cotton swabs moistened with distilled water. In order to provide electrical contacts to the faces of the wafer, an electroless gold solution consisting of 8 drops of Atomex Immersion Gold Solution, 6 drops HF, and 40 ml of distilled water is prepared in a Pyrex beaker. The wafer is placed in this solution and is heated on a hot plate until the surface of the wafer is covered with gold. It is then washed in distilled water, and the flat surfaces are masked with Apiezon Wax W†. The sides are cleaned of any excess wax by using cotton swabs moistened lightly with trichloroethylene. After rinsing the wafer successively with alcohol and distilled water, the gold is

†James G. Biddle Co., Plymouth Meeting, Pennsylvania

removed from the sides with aqua regia, and the crystal is washed in distilled water.

8. Etching and Drift

The wafer is now etched in CP-4A consisting of a 5:3:3 solution of HNO_3, HF, and HOAc in a Teflon beaker. The etching time is 2 1/2 minutes at room temperature. The solution is agitated constantly during etching, and the etch is quenched in distilled water.

After the wafer has been washed free of etchant, it is placed in a beaker of trichloroethylene to remove the Apiezon wax. The wafer is then washed successively in trichloroethylene and alcohol and dried with nitrogen gas.

The reverse current is checked at 100 volts bias, and, if less than 10 μa, the wafer is drifted. If the reverse current is greater than 10 μa, the wafer is left under a reverse bias of 400 volts for approximately 12 hours. If the reverse current at 100 volts is still high after this time, the front and back surfaces are remasked and the wafer is re-etched. If the current is not reduced to 10 μa after a few etches, the trouble is usually attributable to lineage, and the crystal is discarded.

9. Drifting

Three drifting methods,[3,4,6] described in detail by others, have been used with no noticeable differences in the final results. The drift may be stopped at some desired depth, but it is usually continued until the back surface is reached. Some overcompensation or excessive concentration of lithium may occur at the back surface, but, with the stain-etch procedures described in the next section, this presents no problem.

10. Preparation for Final Etch

After drifting, the wafer is lapped to remove the gold and the sides are sanded to remove the etched surface. The crystal is then stain etched, and two effects are observed. The first, shown in Fig. 8, is that the compensated region is stained a tone intermediate between that of the n- and p-type regions. The remainder of the p-type material, in this case the dark, irregular region in the center of the back surface, can be removed by lapping and sanding the surfaces and sides.

The second effect is perhaps the most important for the formation of windowless, surface barrier detectors. As shown in Fig. 8, small circular, darkly stained regions about 50 μ in diameter can be observed on the surface of the crystal in the compensated material. If the back surface is inspected under a low power microscope, it can be seen that the dots are not particularly clear and distinct (Fig. 9). This is the result of the pileup of lithium on the back surface during the drifting process. These regions are usually strongly n-type, and must be removed in order to achieve a windowless detector. The back surface is therefore lapped until sharp, clearly defined dots or circles such as those shown in Figs. 10 and 11 can be observed. In Fig. 10 a screw dislocation, not observable before drift, has become apparent as a result of the lithium-ion compensation. This crystal was discarded since such a dislocation prevents the formation of a good diode structure.

The front surface of the crystal is now lapped and again plated with electroless gold. A flat head stainless steel screw is mounted on the lithium side using DuPont Silver Preparation 8030 which hardens overnight at 30° C. The front surface and the head of the screw are

then masked with Apiezon Wax W. Some care must be taken since the heat required to melt the wax may loosen the screw. However, the silver cement will harden again immediately after cooling. The excess wax is removed from the sides and other faces of the crystal using cotton swabs moistened in trichloroethylene. The crystal is then rinsed in alcohol and distilled water, and the gold is removed from the exposed portion with aqua regia. The wafer is lightly lapped and sanded, and scrubbed with cotton swabs moistened with distilled water.

11. Final Etch

As shown in Fig. 12, the screw is inserted in a plastic pipette in order to hold the crystal in the polish etch. The crystal is etched for 2 1/2 minutes in CP-4A at room temperature, and the etch is again quenched with distilled water. After the etch, the detector is mounted in a Lucite holder as shown in Fig. 13. Gold is evaporated on the face of the detector with the sides of the detector protected by a mask. An ion pump is usually preferred for this vacuum evaporation, since backstreaming of oil onto the detector may occur with oil diffusion pumps.

After evaporation, the detector is stored in darkness for two to three days. The contact to the evaporated gold layer is made with a 0.175 mm gold wire as shown in Fig. 14. A tiny drop of Aquadag[†] is placed on the surface, and the wire is then bent at an angle to contact the detector at this point. A small drop of General Cement Silver Print (with most of the solvent removed) covers the wire at this contact and bonds it to the Aquadag.

[†]Acheson Colloids Co., Port Huron, Michigan

After the contact is dry, the reverse current is measured. In general, the best detectors will have reverse currents less than 1 μa at 100 volts. If the current is higher than this, further storage in darkness under bias voltages of 200-400 volts will occasionally give remarkable improvement. Where the reverse current is very high, and remains so even if the crystal is re-etched, the problem is generally one of lineage in the crystal. It should be emphasized that while low reverse currents are desirable, the change in current with a change in voltage between 100 and 400 volts should also be low and steadily increasing. In fact, for detectors greater than 5 mm in thickness and over 1 cm in diameter, the reverse currents may be as high as 5 μa with detectors whose resolution is quite good. In these cases, an increase in voltage from 100 to 400 volts produces an increase in current of less than 2 μa.

Finished detectors are usually stored in darkness away from excessive heat. If the storage is prolonged, lithium ions will occasionally disappear from the surfaces, and the diode structure may be destroyed. In these cases, good performance may be obtained again by lapping and sanding the crystal, and using stain etching techniques. If the junction between the lithium-rich region and the intrinsic material is restored, and well-formed dots are obtained on the back surface, the crystal can then be etched and finished as before. This has restored good detector properties in almost every case.

The detectors fabricated by these means have resolutions between 15 and 30 keV for the 975 keV conversion line of Bi^{207} when operated at room temperature. For alpha particles, resolutions between 45 and 60 keV on the 8.78 MeV alpha-ray of Mesathorium have been measured. The diameter of the detectors is greater than 1 cm, and the thickness

ranges between 2 and 6 mm. If these detectors are operated at low temperatures, care must be taken not to expose the detector to air while cool since moisture will form on the surface of the detector and may loosen the gold wire contact. These detectors have been used primarily for beta-ray and electron measurements which are described in detail elsewhere.[9-12]

Acknowledgments

The authors are most grateful to J. R. Gigante for his cooperation and assistance at every stage of this work. They have also benefited greatly from the generous advice of H. M. Mann of Argonne National Laboratory.

References

1) J. H. Elliot, Nuclear Inst. and Methods 12 (1961) 60.

2) J. L. Blankenship and C. J. Borkowski, IRE Trans. on Nucl. Sci. NS-9, No. 3 (1962) 181.

3) H. M. Mann, J. W. Haslett, and F. J. Janamek, IRE Trans. on Nucl. Sci. NS-9, No. 4 (1962) 43.

4) G. L. Miller, B. D. Pate, and S. Wagner, IEEE Trans. on Nucl. Sci. NS-10, No. 1 (1963) 220.

5) C. Chasman and J. Allen, Bull. Am. Phys. Soc. 8 (1963) 398.

6) F. S. Goulding and W. L. Hansen, IEEE Trans. on Nucl. Sci. NS-11, No. 3 (1964) 286.

7) R. P. Lothrop and H. E. Smith, UCRL - 16190 (unpublished).

8) C. S. Fuller and J. A. Ditzenberger, J. Appl. Phys. 28 (1957) 40.

9) J. W. Harpster, D. L. Bennett, and K. J. Casper, Nuclear Physics 47 (1963) 443.

10) K. J. Casper and R. H. Thompson, Bull. Am. Phys. Soc. 9 (1964) 17.

11) K. J. Casper and R. H. Thompson, Bull. Am. Phys. Soc. 9 (1964) 688.

12) R. H. Thompson and K. J. Casper, Nuclear Physics (to be published).

Figure Captions

Fig. 1 Silicon wafer after dislocation showing the high dislocation density ring.

Fig. 2 Lapidary wheel used for sanding sides of wafers.

Fig. 3 Schematic drawing of Pyrex diffusion furnace. The diffused area of the crystal is limited by the size of the aperture in the evaporation table.

Fig. 4 Silicon crystal after diffusion in furnace of Fig. 3. The dark inner circle is lithium hydroxide coating and indicates the area of diffusion.

Fig. 5 Diffusion furnace. The heating element is a coil of wire between two stainless steel plates and insulated from them with mica.

Fig. 6 Silicon crystal after diffusion in the furnace of Fig. 5 and after stain etching. The lightly stained regions are the lithium diffused areas, and the darkly stained region is the undiffused p-type material. Diffusion on the sides of the crystal is quite evident.

Fig. 7 Silicon crystal of Fig. 6 after sanding and stain etching. The side diffusion of lithium has been removed, and a sharp, even junction can be seen.

Fig. 8 Back surface of silicon crystal after drifting. The dark area is the uncompensated p-type material.

Fig. 9 Back surface of silicon crystal, after drifting as seen under a low-power microscope. The dots are rather blurred and indistinct.

Figure Captions (continued)

Fig. 10 Back surface of silicon crystal of Fig. 9 after additional lapping and stain etching.

Fig. 11 Surface of Fig. 10 as seen under a low-power microscope. The dots and circles should be compared to Fig. 9 to note the improvement in sharpness.

Fig. 12 Detector mounted in plastic pipette shown just after the final polish etch.

Fig. 13 Schematic drawing of detector showing method of mounting.

Fig. 14 Finished detector with top contact shown.

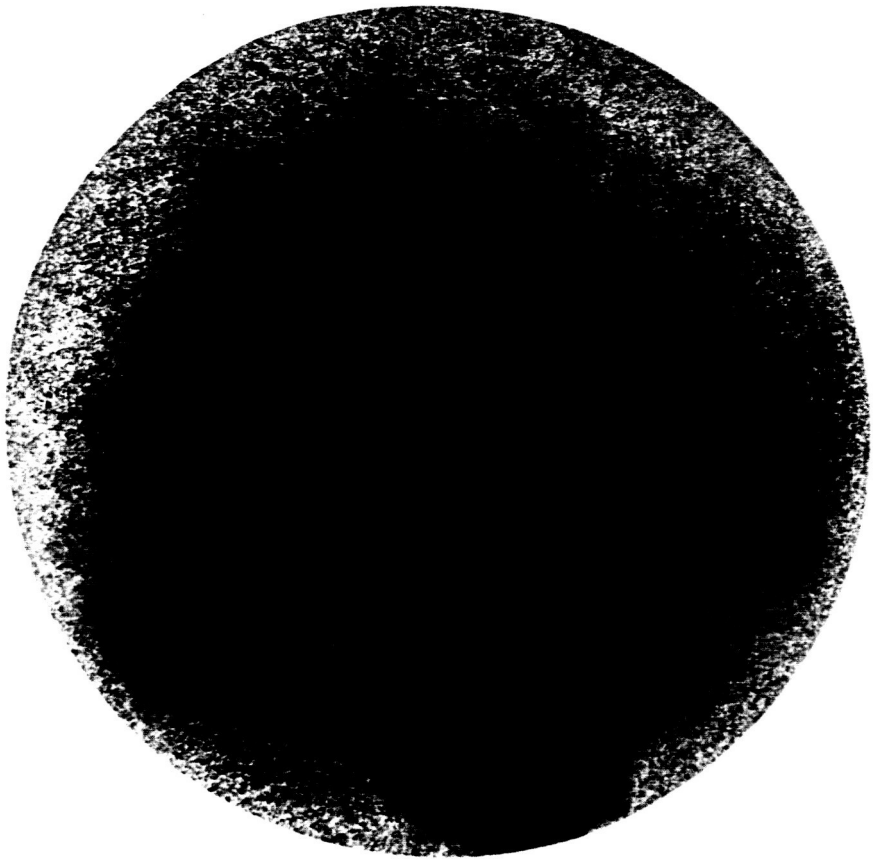

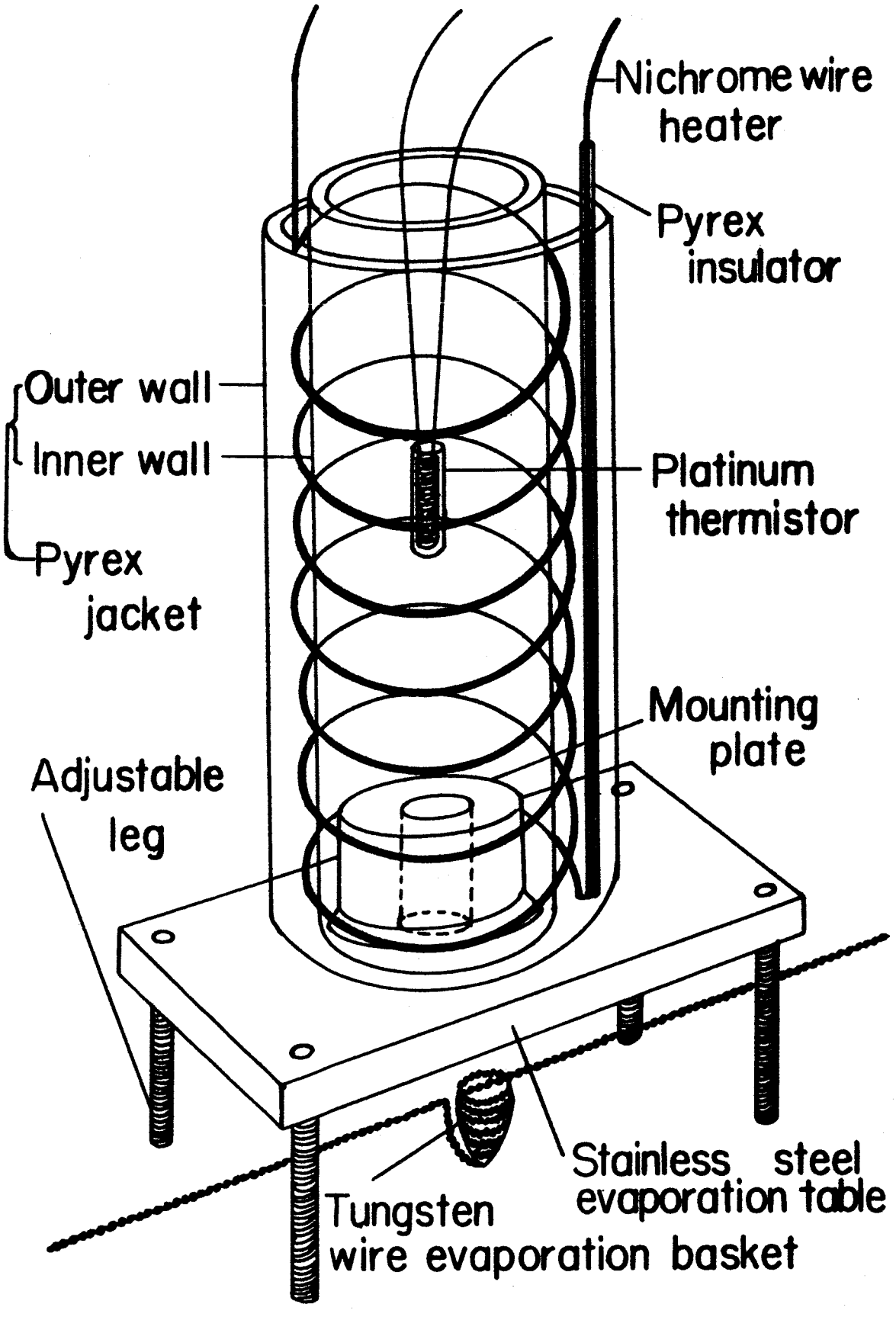
Nichrome wire heater
Pyrex insulator
Outer wall
Inner wall
Pyrex jacket
Platinum thermistor
Mounting plate
Adjustable leg
Stainless steel evaporation table
Tungsten wire evaporation basket

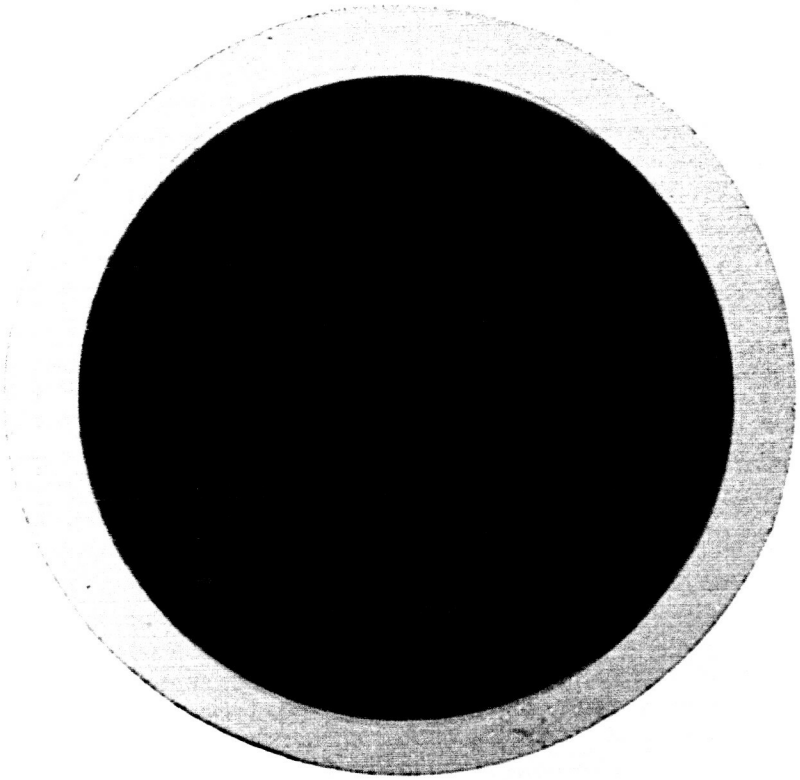

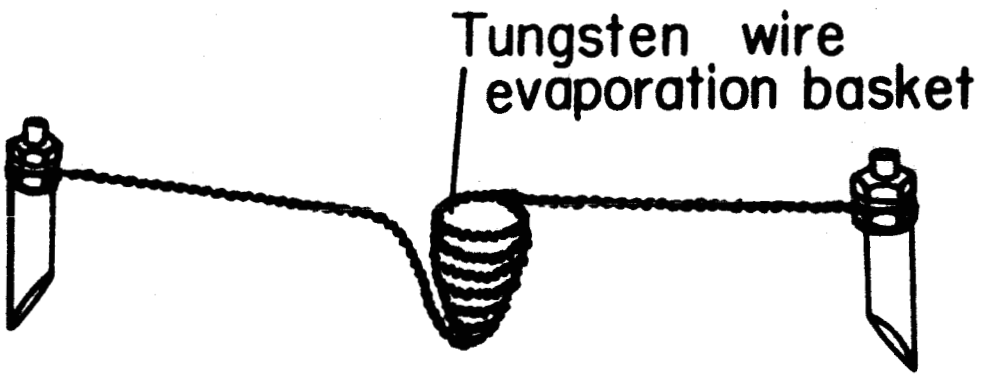
Tungsten wire
evaporation basket

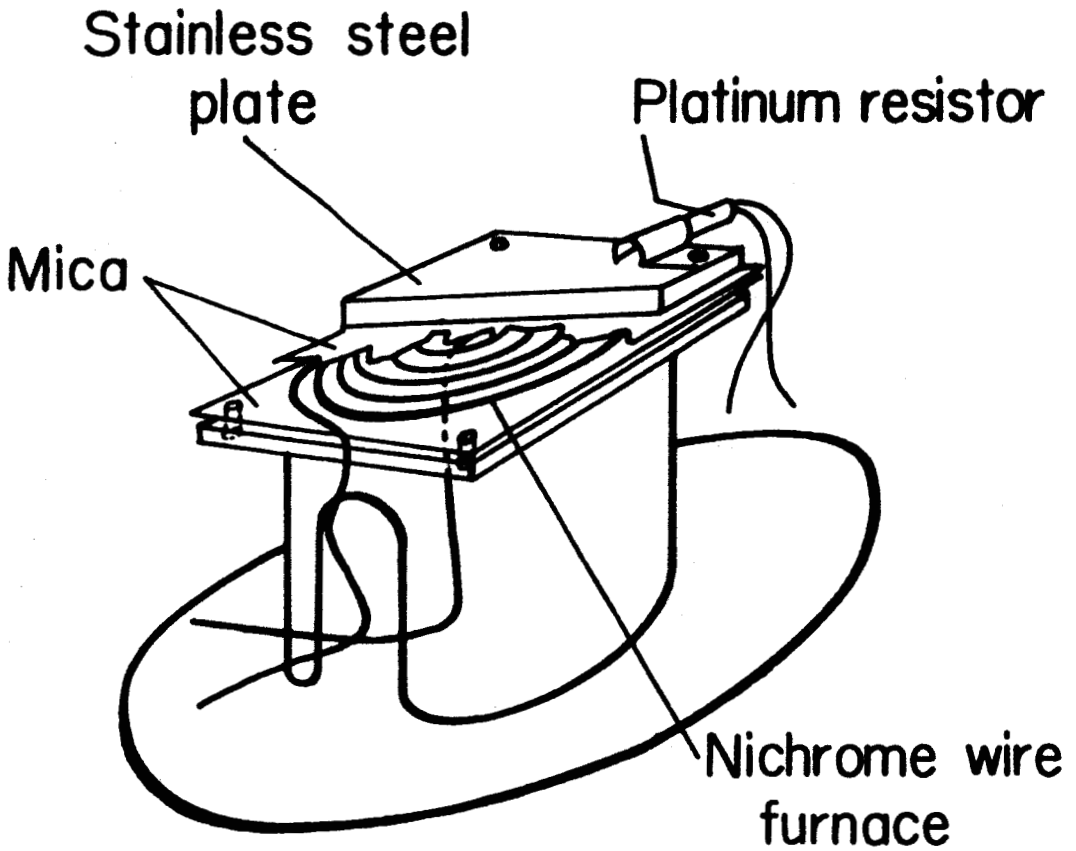
Stainless steel
plate
Platinum resistor
Mica
Nichrome wire
furnace

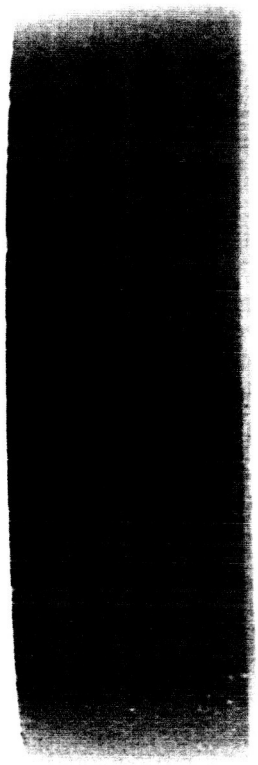

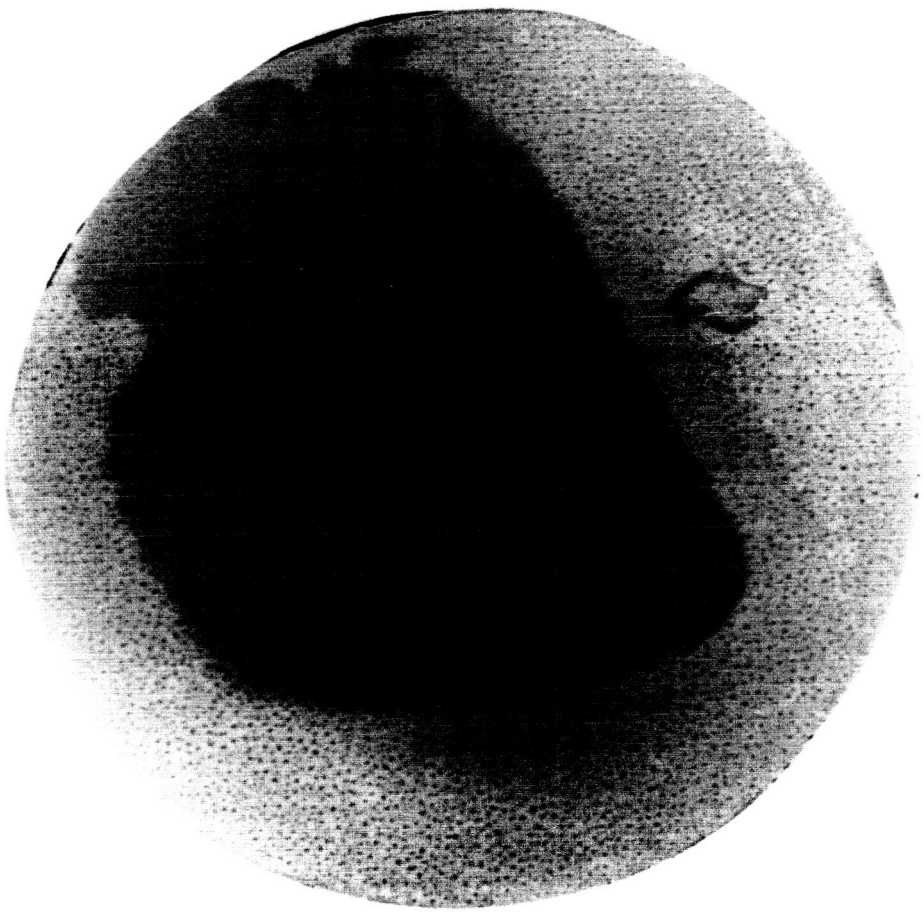

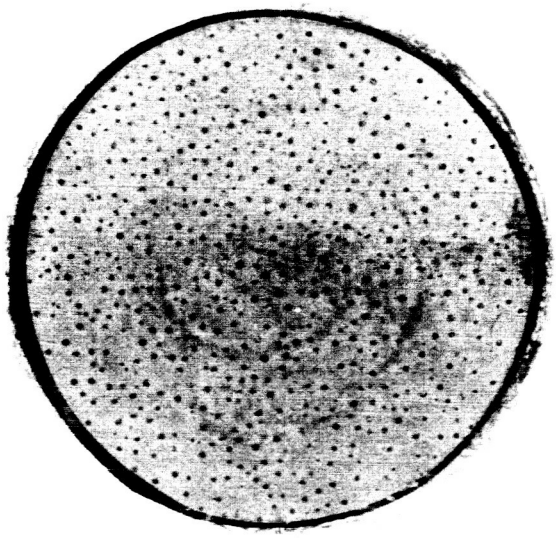

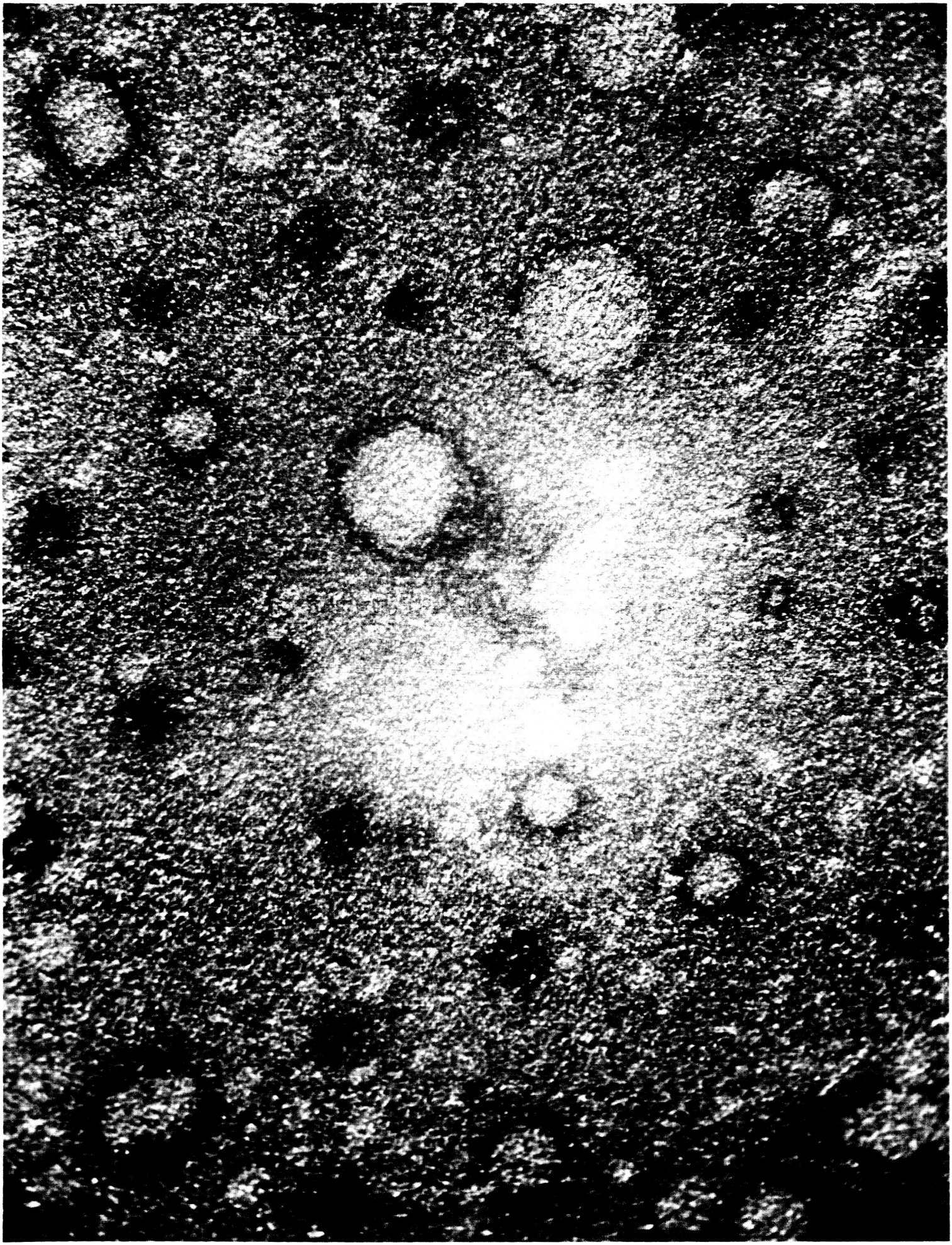

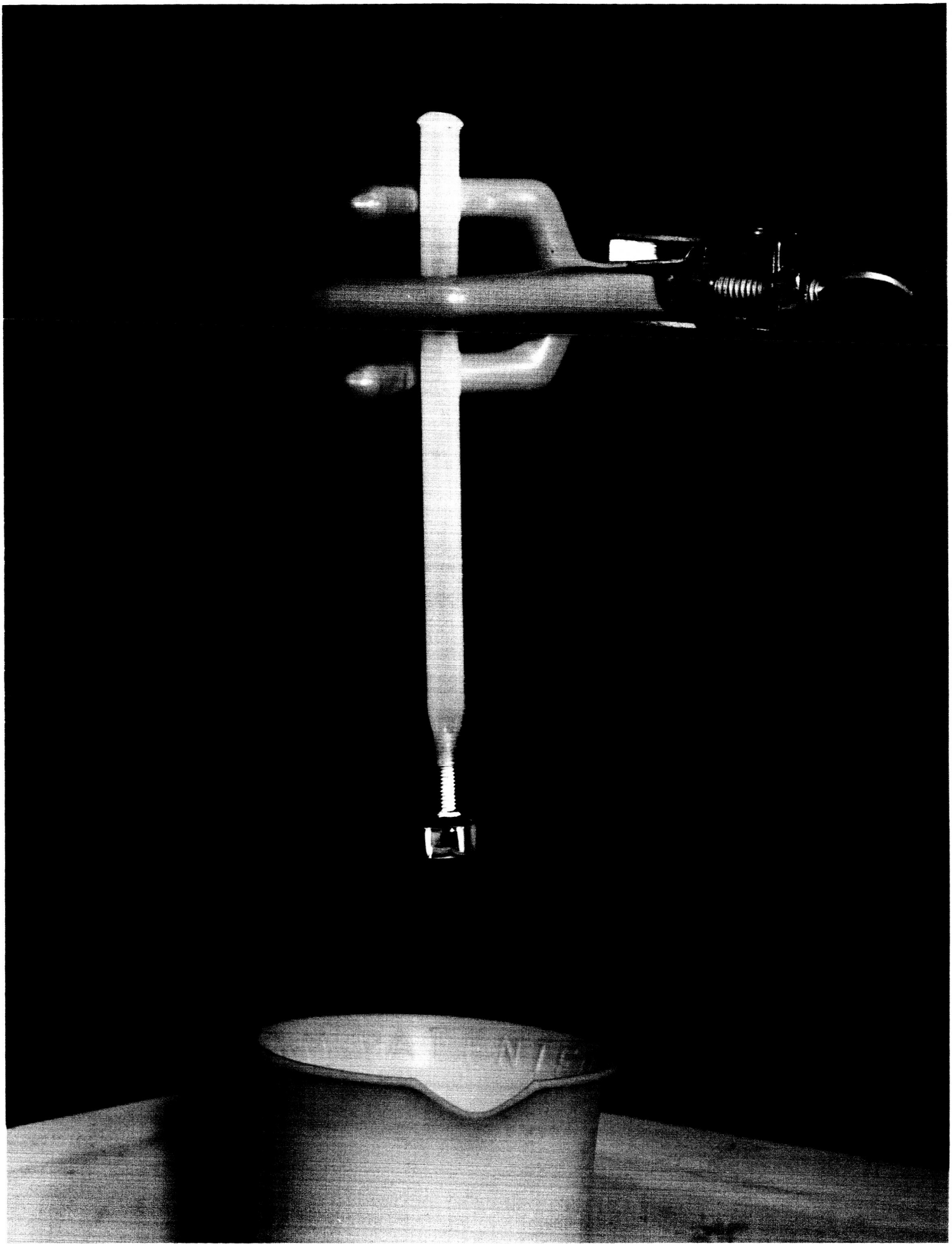

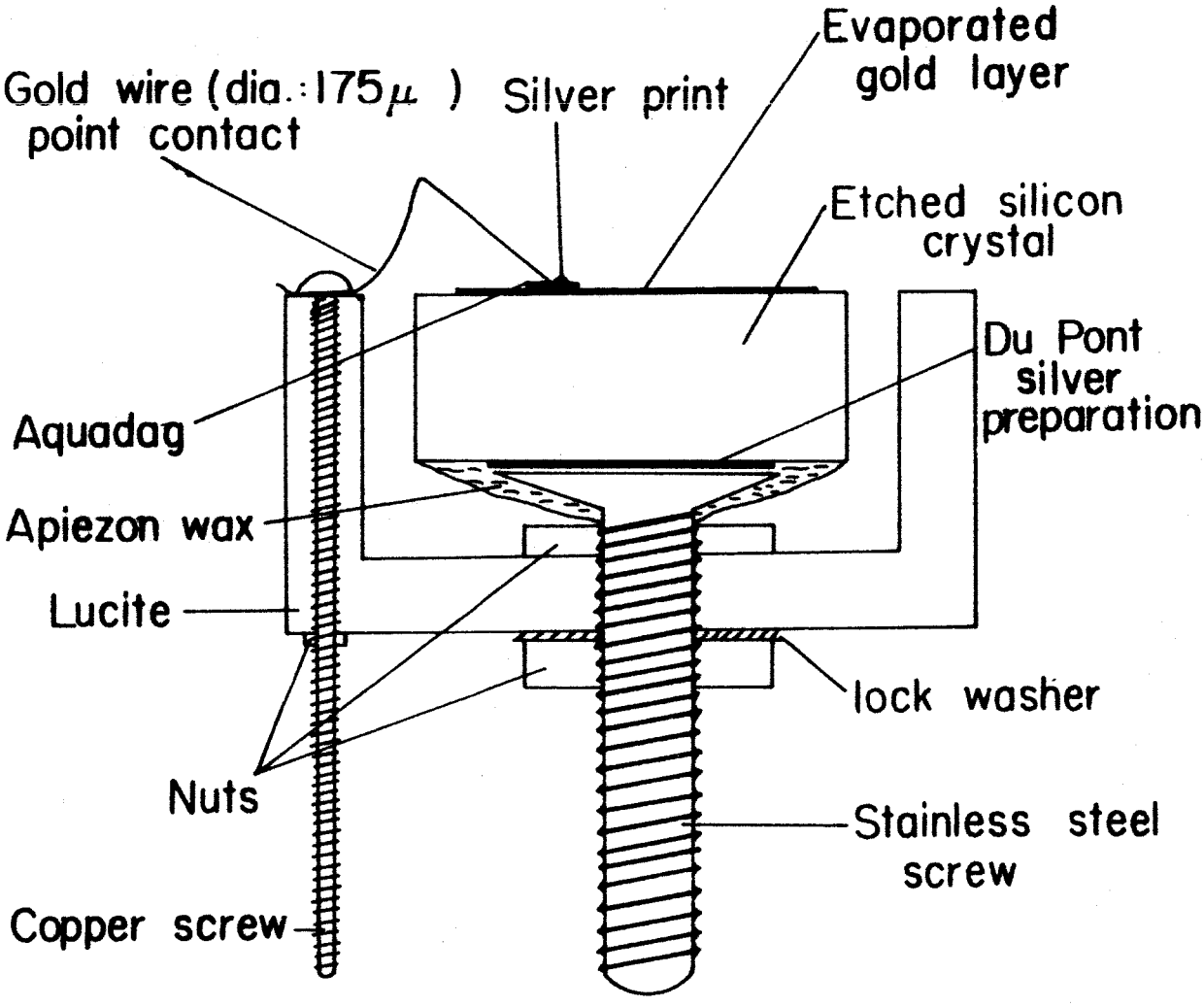
Gold wire (dia.: 175μ) point contact
Silver print
Evaporated gold layer
Etched silicon crystal
Du Pont silver preparation
Aquadag
Apiezon wax
Lucite
lock washer
Nuts
Stainless steel screw
Copper screw

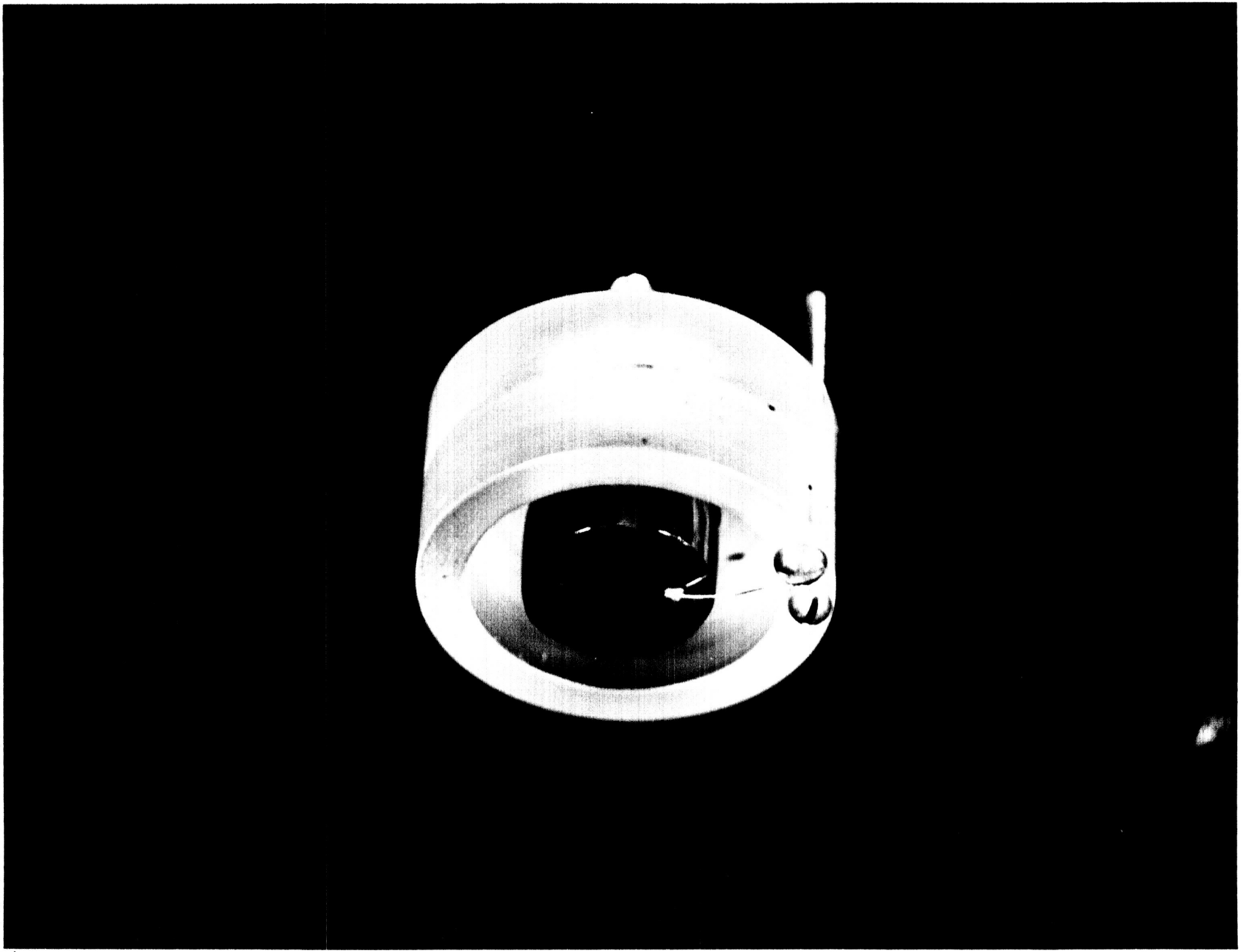

N66-15634

COMPUTER PROGRAM FOR ANALYSIS OF BETA-RAY SPECTRA MEASURED WITH SOLID STATE DETECTORS

Introduction

This paper describes in detail the Fortran IV program previously used[1] for the analysis of beta-ray spectra measured with lithium drifted surface barrier silicon detectors. The program consists of the following major subdivisions:

(1) Fitting of the measured spectrum with a Tchebycheff polynomial.

(2) An iteration procedure using the measured response function of the detector in order to extract the true, undistorted spectrum from the measured spectrum.

(3) Computation of the Fermi-Kurie plot using the shape correction factor is necessary and determination of the endpoint energy by least squares fit.

Description of the program

To understand the necessity for this program, it must be realized that solid state silicon detectors do not produce a constant amplitude pulse for all monoenergetic electrons which are incident upon it. If the detector is thick enough so that the range of the particles is less than the thickness, then there are three main reasons for this phenomena:

1) The detector has a finite energy resolution.

2) There is incomplete energy loss by the incident particles as a result of backscattering from the face of the crystal. There may also be some incomplete energy loss as a result of electrons

emerging from the sides of the crystal either by virtue of a large angle scattering or of the initial angle of incidence.

3) As a result of the physical characteristics of the crystal such as the lifetime, mobility, recombination centers, non-uniform electric field distribution, not all of the ion pairs which are created may be collected.

All of these factors may be taken into account in the analysis of data simply by measuring the spectra of monoenergetic electrons of varying energy. This may be done rather simply with a beta-ray spectrometer. However, internal scattering of electrons from the baffles can introduce some distortion in the spectrum, and some care must be taken in interpreting the data. In general, the response function is assumed to have the simple shape shown in Fig. 1.

The response function has a very strong dependence upon energy. To specify this dependence, a parameter, A_p/A_t, the ratio of the number of counts under the peak to the total area under the entire curve is defined. This is simply the relative number of counts whose energy is measured correctly. For computational purposes it is necessary to fit this parameter in an analogue fashion. Thus, for the typical curve shown in Fig. 2, the low energy end of the curve is approximated by an exponential, $e^{-\alpha(W + \beta)}$, and after some point, W_t, called the transition energy, the curve is fitted by a straight line. MW + B, where W is the total electron energy. The parameters α, β, M and B are deterined experimentally, and may be quite different for different detectors.

The program itself is appended to this paper. The dimension statements assign 400 storage positions since 400 channel analyzer was used.

The format statements are used for the following purposes:

300 This statement is used to read in the first (IO) and last (IL) channel numbers.

301 This is used for the actual data.

302 This is a heading which states what nucleus is being studied. The Z and A of the nucleus must be supplied on a data card. The second part of the heading introduces a table of data with the background counts subtracted from the data.

303 This statement is used to print out the table of 302 and other tables at various stages of the program.

304 This statement is used to read in IREPL, the number of iterations used in obtaining the undistorted spectrum, RESOL, a number equal to twice the resolution of the detector expressed in number of channels, WW, the energy of the first channel, BET2, the energy difference between channels, IK, a channel number introduced if various branches are to be analyzed and one does not wish to analyze below some point, CHART, a number used to label the particular run.

305 This statement is used to read in the Z and the A of the nucleus. It also reads in WO, an estimate of the end point energy if a shape correction factor is used or zero if the spectrum is assumed to have an allowed shape, IST, the first channel used in the Fermi-Kurie plot and, ILST, the last channel used in the Fermi-Kurie plot.

306 This is a heading which labels the Tchebycheff fitted data and gives the number of iterations used in the fit.

307 This statement is used to print the resolution of the detector, CHART, WW, BET2, and IK.

308 This statement is used to identify the coefficients which are used to fit A_p/A_t as a function of W. RALPH is α, RTRAN is the transition channel where the exponential fit changes to a straight line fit, RM and RB are the M and B parameters respectively.

310 This statement is used to label a table of the data after the iterations. Two tables are printed out. The first contains the data after the first iteration and the second contains the data after the last iteration.

311 This statement is used to label a table which contains data for the Fermi-Kurie plot.

312 This statement is used to print out the data for the heading and table of the Fermi-Kurie plot.

313 This statement is used to print the results of the least squares fit of the Fermi-Kurie plot, that is the coefficients a and b of the straight line fit, aW + b, WC(0), the endpoint energy from the straight line fit, and DELY, a weighted average of the error of the fit.

314 and 315 These statements are used to print out some of the calculations of the least squares fit, primarily for purposes of checking the fit.

Statements 1 through 2 of the program are used to read in data. Statements 3 through 7 insure that there are an odd number of data points and subtract out the background. Statements 8 through 11 take the square

root of the data, so that the numbers to be handled by the Tchebycheff subrouting will be within the range of the computer.

At this point the Tchebycheff subroutine is called and the data is fit with a smooth curve using Tchebycheff polynomials. This is done simply to prevent the iteration process from magnifying small statistical fluctuations into large peaks and valleys. The advantage of using Tchebycheff polynomial series rather than simple power series is that the coefficients remain unchanged regardless of the number of terms that are added to the expansion. With a simple power series, the addition of a higher term means that each coefficient of each term must be recalculated. This subroutine is listed at the end of the program and follows the methods of Birge and Weinberg.[2]

After the polynomial fit, the points of the smoothed curve are squared to obtain a smooth curve fit to the original data points. This is accomplished in statements 12 through 17.

At this point the true spectrum is extracted using the detector response function. The basic method of this part of the program is relatively simple. The measured spectrum is essentially the true spectrum spread out by the response function of the detector. Therefore, with the measured spectrum as a starting point, the true spectrum is estimated. This estimated true spectrum is then spread out by the detector response function and compared with the measured spectrum. If there is agreement, then the estimated true spectrum and the true spectrum are the same. If there is no agreement, the estimated true spectrum is adjusted in some consistent fashion. After this adjustment, the new spectrum is spread out by the

detector response function and compared with the measured spectrum. This self-consistent calculation is continued until the desired agreement is obtained.

The first step is to find some way of estimating the true spectrum. The measured spectrum is related to the true spectrum by[3]

$$N_m(W) = \int_1^{W_o} N_t(W')L(W,W')dW' \qquad (1)$$

where $N_m(W)$ is the measured counting rate at some energy W, N_t is the true (undistorted) counting rate at W', and L(W,W') is the fraction of the number of electrons of energy W' incident on the detector which are observed as having energy W. The simplest approach is to assume that the measured spectrum is the true spectrum and to make the substitution $N_m(W') = N_t(W')$ in Eq. 1. A measured spectrum $N_m'(W)$ is obtained. An estimate to the true spectrum is then obtained by substituting this new spectrum into the equation

$$N_t'(W) = N_m(W) - [N_m'(W) - N_m(W)] \quad . \qquad (2)$$

Basically, this approximation amounts to assuming that the measured spectrum is spread out by the same amount that the true spectrum was spread out. Therefore, by simply adding back in the differences to the original measured spectrum we should obtain the true spectrum. This is obviously not quite correct, Therefore, the "true" spectrum $N_t'(W)$ is substituted into Eq. 1,

the result is compared in Eq. 2, and the next approximation $N_t''(W)$ obtained. The process is continued until the desired agreement is obtained. This procedure is carried out in the program in steps 17 through 33.

As an example of how this part of the program works, taken any point N_i. Since the detector has a finite energy resolution, these counts will be spread over a triangular peak whose base is twice the resolution of the detector and whose height N_{2i} is given by

$$N_{2i} = N_i(2/\Delta)(A_p/A_t)_i$$

where Δ is the base width in channels.

Many of the counts from this peak are distributed over a constant amplitude tail, whose height is given by

$$N_{3i} = N_{2i}[(A_t/A_p) - 1]_i/[(2/\Delta)(I0 + i - 1) - 1]$$

where I0 is the first channel. These two amplitudes are calculated in the steps just preceding statement 22.

Now to the counts in the ith channel must be added all the contributions from the backscatter tails of the higher energy peaks. This is accomplished in steps 22 through 25. The contributions due to the finite resolution of the peaks on either side of the ith peak are now added to N_i. These contributions are given by SUM2 in step 30. Steps 31 and 32 correspond to equation 2. It has been found simplest to perform a number of iterations and visually examine the results to determine the point at which the iteration is stopped.

The Fermi-Kurie plot is calculated in steps 35 through 47. As part of this plot, the complex gamma function is calculated with a subprogram and the exact Coulomb factors are also calculated. Finally, in the remainder of the program a least-squares fit of the Fermi-Kurie plot is made, and the errors are calculated.

REFERENCES

1. R. H. Thompson and K. J. Casper, Nuclear Physics (to be published).

2. R. M. Birge and J. W. Weinberg, Rev. Mod. Phys. 19 (1947) 298.

3. M. S. Freedman, T. B. Novey, F. T. Porter, and F. Wagner, Jr., Rev. Sci. Inst. 27 (1956) 716.

FIGURE CAPTIONS

Fig. 1 Simple shape assumed for response function.

Fig. 2 A_p/A_t for a typical detector as a function of electron energy W.

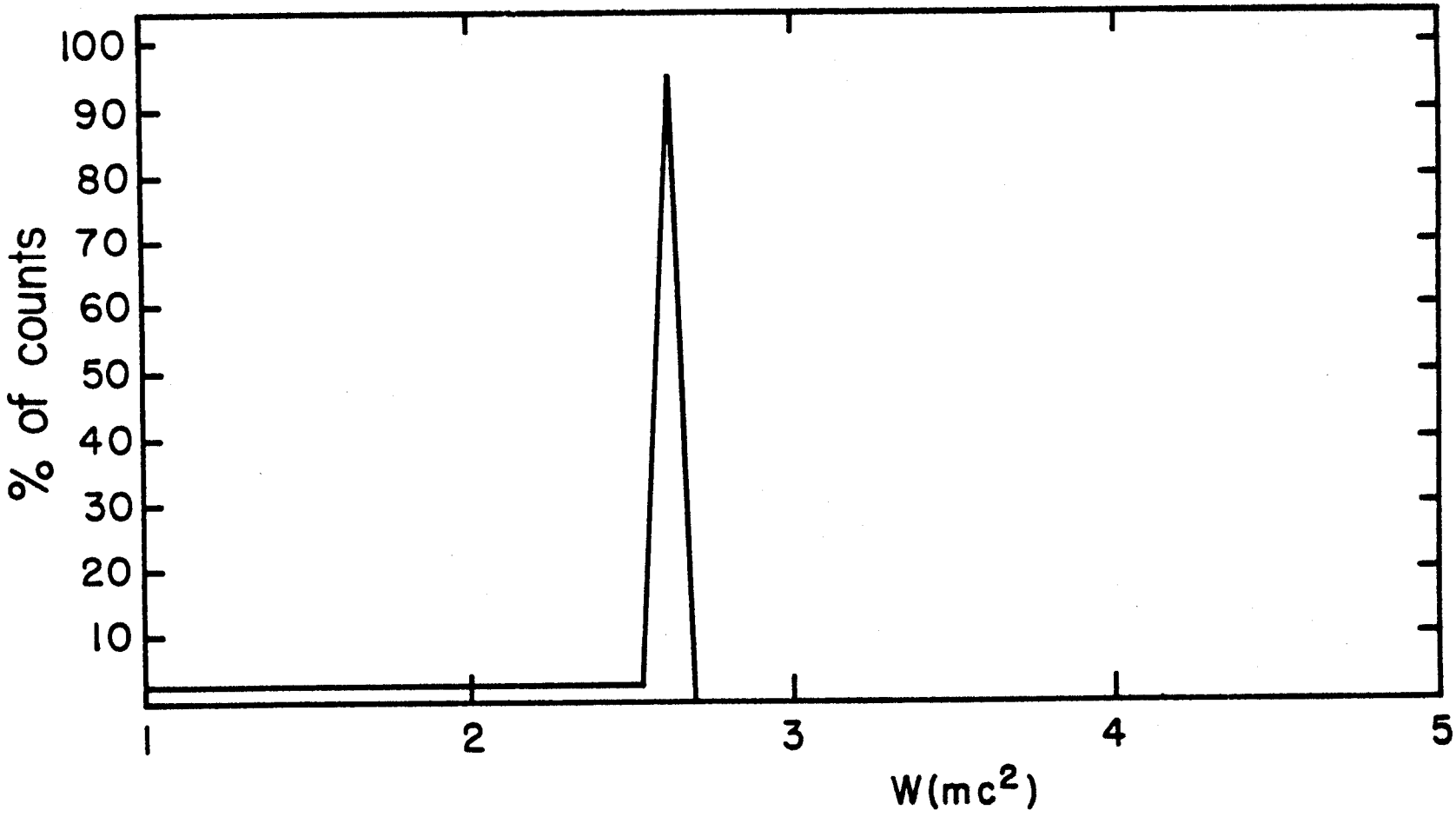
100
90
80
70
60
50
40
30
20
10
% of counts
1
2
3
4
5
W(mc²)

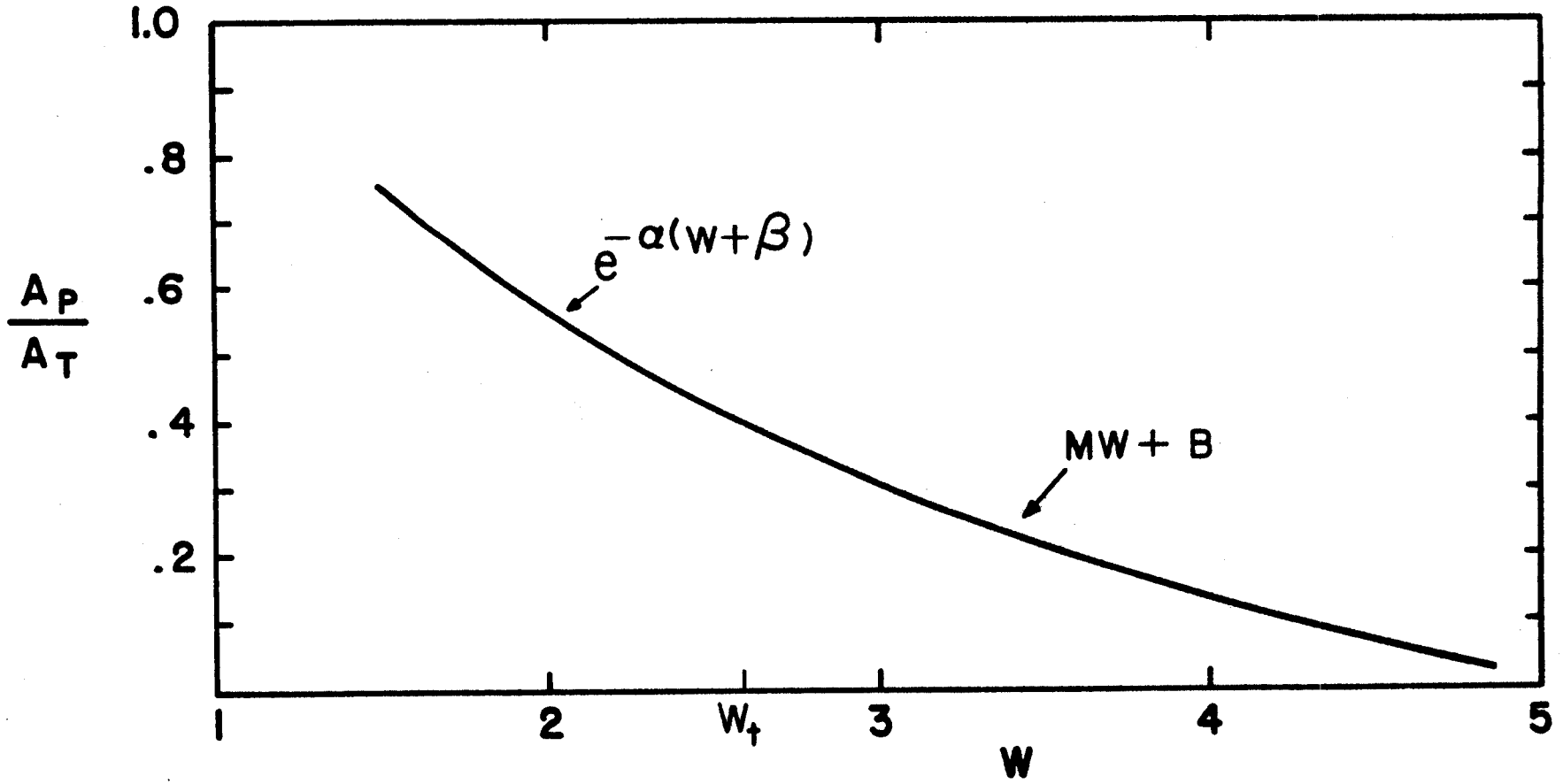
1.0
.8
.6
.4
.2
$\frac{A_P}{A_T}$
$e^{-\alpha(W+\beta)}$
MW + B
1
2
W_t
3
4
5
W

```
-A  FOR  TCH
      DIMENSION RN (400),RN5(400)
      DIMENSION RN4(400),W(400),RATIO(400),RN2(400),RN3(400)
  300  FORMAT (8I10)
  301  FORMAT (8F10.0)
  302  FORMAT (42H1TCHEBYCHEFF POLYNOMIAL FIT, ETC., FOR Z =,F6.1,3X,
     1 3HA =,F7.1/76H0ORIGINAL DATA, WITH SMALLEST COUNT LESS 1 SUBTRACT
     2ED, STARTING WITH CHANNEL,I4)
  303  FORMAT (1X,10F11.1)
  304  FORMAT (I10,3F10.0,I10,F10.0)
  305  FORMAT (3F10.0,2I10)
  306  FORMAT (30H0TCHEBYCHEFF RESULTS OF DEGREE,I4)
  307  FORMAT (13H0RESOLUTION =,F6.3,3X,7HCHART =,F10.7,3X,4HWW =,F10.6,
     1 3X,6HBET2 =,F10.6,3X,4HIK =,I4)
  308  FORMAT (31H0AP/AT COEFFICIENTS ARE ALPHA =,F10.6,10X,9HFOR W GEQ,
     1 F6.2,2X,7HARE M =,F12.6,2X,3HB =,F12.6)
  309  FORMAT (1X,12F10.5)
  310  FORMAT (43H0COUNTS, AFTER CORRECTIONS OF ITERATION NO.,I3,27H ARE,
     1 STARTING WITH CHANNEL,I4)
  311  FORMAT (11H1SHAPE W0 =,F10.6,3X,5HIST =,I5/8H0CHANNEL,4X,2HWC,8X,
     1 5HFERMI,6X,5HSHAPE,7X,6HLAMBDA)
  312  FORMAT (1X,I5,3F11.6,F13.6,2F11.6)
  313  FORMAT (10H0LINE, A =,F9.5,3X,3HB =,F9.5,3X,7HWC(0) =,F10.6,3X,
     1 7HDEL-Y =,F10.6)
  314  FORMAT (1H0,I5,5F13.5)
  315  FORMAT (15H0DELTA LAMBDA =,F11.3,3X,4HSY =,F11.4,3X,4HSA =,F11.4,
     1 3X,4HSB =,F11.5)
    1   READ 300, I0,IL
        IF (IL.EQ.0) STOP
        K = IL - I0 + 1
```

```
      READ 301, (RN(I),I = 1,K)
      READ 304, IREPL,RESOL,WW,BET2,IK,CHART
      READ 305, Z2, A2, W0, IST, ILST
      READ 301, RALPH, RTRAN, RM, RB
2     PRINT 302, Z2,A2,I0
3     TSTA = K/2.0
      I = TSTA
      IF (TSTA - I - 0.0005) 4,5,5
4     K = K - 1
      IL = IL - 1
      IF (IL.LT.ILST) ILST = IL
5     TSTA =RN(K)
      J = K - 10
      DO 6 I = J,K
      IF (RN(I).LT.TSTA) TSTA = RN(I)
6     CONTINUE
      TSTA = TSTA - 1.0
      DO 7 I = 1,K
7     RN(I) = RN(I) - TSTA
8     PRINT 303, (RN(I), I = 1,K)
      DO 11 I = 1,K
      RN5(I) = RN(I)
      IF (RN(I)) 9,10,10
9     RN(I) = -SQRT (-RN(I))
       GO TO 11
10    RN(I) = SQRT (RN(I))
11    CONTINUE
      PRINT 307, RESOL,CHART,WW,BET2,IK
      PRINT 308, RALPH,RTRAN,RM,RB
      CALL TCHEB (RN,I0,IL,ITL)
12    DO 15 I = 1,K
```

```
      IF (RN(I)) 13,14,14
   13 RN(I) = -RN(I)*RN(I)
      GO TO 15
   14 RN(I) = RN(I)*RN(I)
   15 CONTINUE
      PRINT 306, ITL
   16 PRINT 303, (RN(I), I = 1,K)
   17 IADD = (RESOL - 0.5)/2.0
      IP = IO-IK -1
      DO 20 I = 1,K
      W(I) = WW+BET2*(I+IP)
      RATIO(I) = EXP (-RALPH*(W(I)-1.0))
      IF (W(I).GT.RTRAN) RATIO(I) = RM*W(I) + RB
   20 RN4(I) = RN(I)
   21 DO 33 IREP = 1,IREPL
      TSTA = 2.0/RESOL
      SUM1 = 0.0
      RN1 = RN(1)
      RNK = RN(K)
      DO 22 I = 1,K
      RN2(I) = RN(I)*TSTA*RATIO(I)
      RN3(I) = RN2(I)*(RESOL/(2.0*(IO+I-1) - RESOL))*(-1.0+1.0/RATIO(I))
   22 SUM1 = SUM1 + RN3(I)
      DO 23 I = 1,IADD
   23 SUM1 = SUM1 - RN3(I)
      DO 32 I = 1,K
      IADDP = I + IADD
      IADDM = I - IADD
      IF (IADDP +1 - K) 25,25,24
   24 SUM1 = 0.0
      GO TO 26
```

```
25    SUM1 = SUM1 - RN3(IADDP)
26    SUM2 = 0.0
      TSTA = 2.0*(I0+I-1)
      DO 31 J = IADDM,IADDP
      IF (J) 27,27,28
27    SUM2 = SUM2 + (RESOL - ABS(2.0*(I0+J-1)-TSTA))*RN1*2.0*EXP (-RALPH
     1 *(-1.0+(WW+BET2*(J+IP)))) / (RESOL*RESOL)
      GO TO 31
28    IF (J.EQ.I) GO TO 31
      IF (J-K) 30,30,29
29    SUM2 = SUM2 + (RESOL - ABS(2.0*(I0+J-1) - TSTA))*RNK*2.0*(RB+RM*
     1 (WW+BET2*(J+IP)))/(RESOL*RESOL)
      GO TO 31
30    SUM2 = SUM2 + (RESOL - ABS(2.0*(I0+J-1) - TSTA))*RN2(J)/RESOL
31    CONTINUE
      TSTA = RN4(I) - RN2(I) - SUM1 - SUM2
32    RN(I) = RN(I) + TSTA
      IF((IREP.NE.IREPL) .AND. (IREP.NE. 1))GO TO 33
      PRINT 310, IREP,I0
      PRINT 303, (RN(I), I = 1,K)
33    CONTINUE
35    ALPH2=0.0072972
      PI = 3.141593
      ALPHZ = Z2*ALPH2
      GAM2 = SQRT (1.0-ALPHZ*ALPHZ)
      GAM3=SQRT(4.0-ALPHZ*ALPHZ)
      R2=(CBRT(A2))*ALPH2
      POW = 2.0*(GAM2-1.0)
      POT=2.0*(GAM3-GAM2-1)
      FERM2 = 2.0*(1.0+GAM2)
      FERM3=2.0+GAM3
```

```
      TSTA = 2.0*GAM2+1.0
      GAMD = CGAM (TSTA,0.0)
      GAMD = EXP (2.0*GAMD)
      GOME=144.0*GAMD
      TSTB=1.0+2.0*GAM3
      GAME=CGAM(TSTB,0.0)
      GAME=EXP(2.0*GAME)
   40 WOSQ = W0*W0
      PRINT 311,W0,IST
      SUML = 0.0
      SUMW = 0.0
      SUMWW = 0.0
      SUMLW = 0.0
      SUMLL = 0.0
      SUMDL = 0.0
      K = ILST - IST + 1
      DO 47 I = I0, ILST
      WC = W (I+1-I0)
      P2 = SQRT (WC*WC - 1.0)
      Y2 = ALPHZ*WC/P2
      GAMN = CGAM (GAM2,Y2)
      GAMN = EXP (2.0*GAMN)
      GAMM=CGAM(GAM3,Y2)
      GAMM=EXP(2.0*GAMM)
      FERMC=FERM2*((R2*P2)**POW)*(EXP(PI*Y2))*GAMN/GAMD
      IF (W0.LT.0.0000001) GO TO 41
      RLAMB2=(FERM3/FERM2)*((R2*P2)**POW)*(GOME/GAME)*(GAMM/GAMN)
      SHAPC = 0.083333333*(WOSQ - RLAMB2) - 0.1666667*W0*WC +
     1 0.083333333*(1.0+RLAMB2)*WC*WC
      GO TO 42
   41 SHAPC = 1.0
```

```
42    J = I - I0 + 1
      IF (RN4(J)) 44,43,44
44    MPR = RN5(J)*RN(J)/RN4(J)
      IF (MPR) 45,46,46
45    IF (SUMWW.LT.0.0000001) GO TO 1
43    K = K - ILST + I - 1
      GO TO 48
46    TSTB = 1.0/(P2*WC*FERMC*SHAPC)
      RLAMB3 = SQRT (MPR*TSTB)
      DLAMB = 0.5*TSTB
      IF (I.LT.IST) GO TO 47
      SUML = SUML + RLAMB3
      SUMLL = SUMLL + RLAMB3*RLAMB3
      SUMW = SUMW + WC
      SUMWW = SUMWW + WC*WC
      SUMLW = SUMLW + WC*RLAMB3
      SUMDL = SUMDL + DLAMB*DLAMB
47    PRINT 312, I, WC, FERMC, SHAPC, RLAMB3
48    WBAR = SUMW/K
      RLBAR = SUML/K
      B2 = (SUMLW - WBAR*SUML)/(SUMWW - WBAR*SUMW)
      TSTA = RLBAR - B2*WBAR
      WX = -TSTA/B2
      DELY = SQRT (SUMDL/(K-2))
      PRINT 313, TSTA,B2,WX,DELY
      PRINT 314, K,SUMW,SUML,SUMWW,SUMLW,SUMLL
      SLSQU = SUML*SUML
      SWSQU = SUMW*SUMW
      SLWSQ = SUMLW * SUMLW
      TSTA = K*SUMWW - SWSQU
      DELL = SUMLL - ((SLSQU*SUMWW - 2.0*SUMLW*SUMW*SUML+K*SLWSQ)/TSTA)
```

```
      SY = SQRT (DELL/(K-2.0))
      SA = SY*SQRT (SUMWW/TSTA)
      SB = SY*SQRT (K/TSTA)
      PRINT 315, DELL,SY,SA,SB
      GO TO 1
      END
```

-A FOR CGAM

```
      FUNCTION CGAM (X,Y)
      REAL I9ZLN
      IF (X - 10.0) 2,1,1
 1    XP = X
       GO TO 3
 2    I = X
      TSTA = X - I
      XP = 9.0 + TSTA
 3    YSQ = Y*Y
      TSTB = XP*XP + YSQ
      R9ZLN = 0.5*ALOG(TSTB)
      I9ZLN = ATAN (Y/XP)
      TSTA = XP - 0.5
      CGAM = TSTA*R9ZLN - Y*I9ZLN - XP + 0.9189385 + XP/(12.0*TSTB)
      TSTA = 1.0
      TSTB = X
 4    IF (XP - 0.0005 -TSTB) 6,5,5
 5    TSTA = TSTA*(TSTB*TSTB + YSQ)
      TSTB = TSTB + 1.0
      GO TO 4
 6    CGAM = CGAM - 0.5*ALOG(TSTA)
      RETURN
```

```
      END


-A  FOR  TCHEB
      SUBROUTINE TCHEB (RN,IO,IL,ITL)
C  TCHEBYCHEFF POLYNOMIAL FIT, USING HIGHEST DEGREE LEQ 18 THAT WON-T GO
C  OUT OF RANGE.  IF THERE ARE AN EVEN NO. OF POINTS, LAST POINT WILL
C  BE THROWN OUT AND IL CHANGED ACCORDINGLY
      REAL M0,M
      DIMENSION RN(400),C(20),M(20),A(20),R(20),T(20),TS(400,20)
  300 FORMAT (26HCCS, STARTING WITH C1, ARE/(1X,8E14.6))
  301 FORMAT (43HOMS DIVIDED BY ACCUMULATIVE 10 TO THE POWER,I3,
     1  22H ARE, STARTING WITH M0,/(1X,8E14.6))
  302 FORMAT (26HOAS, STARTING WITH A0, ARE/(1X,8E14.6))
  303 FORMAT (26HORS, STARTING WITH R0, ARE/(1X,8E14.6))
      K = IL - IO + 1
      TSTA = K/2.0
      I = TSTA
      IF (TSTA - I - 0.0005) 1,2,2
    1 K = K - 1
      IL = IL - 1
    2 EMAX = (K - 1.0)/2.0
      IMAX = EMAX + 0.0005
      M0 = K
      M0SQ = M0*M0
      TSTA = (M0SQ - 1.0)/12.0
      ROSUM = 0.0
      A0 = 0.0
      ICT = 0
      IEXP = 2
      TSTB = TSTA/1000.0
```

```
      IF (TSTB.GE.1.0) IEXP = 3
      IF (TSTB.GE.10.0) IEXP = 4
      IF (TSTB.GE.100.0) IEXP = 5
      IF (TSTB.GE.1000.0) IEXP = 6
      ITL = 37.0/IEXP
      DO 3 J = 1,ITL
      A(J) = 0.0
3     C(J) = (J*J*(MOSQ - J*J))/ (16.0*J*J - 4.0)
      PRINT 300, (C(J), J = 1,ITL)
      TSTA = 10.0**(-IEXP)
      M(1) = C(1)*M0*TSTA
      DO 4 I = 2,ITL
4     M(I) = C(I)*M(I-1)*TSTA
      PRINT 301,IEXP,M0,(M(I),I = 1,ITL)
      IMAX1 = IMAX + 1
      DO 12 L = 1,IMAX1
      EPS = L - 1.0
      IP = L + IMAX
      IM = IMAX + 2 - L
      T0 = 1.0
      T(1) = EPS
      T(2) = EPS*T(1) - C(1)
      DO 5 I = 3,ITL
5     T(I) = EPS*T(I-1) -C(I-1)*T(I-2)
      DIFF = RN(IP) - RN(IM)
      SUM = RN(IP) + RN(IM)
      ROSUM = ROSUM + RN(IP)*RN(IP)+RN(IM)*RN(IM)
      IF (IP - IM) 7,6,7
6     ROSUM = ROSUM - RN(IP)*RN(IP)
      DIFF = RN(IP)
      SUM = DIFF
```

```
 7      A0 = A0 + SUM
        DO 8 I = 1,ITL,2
 8      A(I) = A(I) + DIFF*T(I)
        DO 9 I = 2,ITL,2
 9      A(I) = A(I) + SUM*T(I)
        ICT = ICT + 1
        DO 10 I = 1,ITL
 10     TS (ICT,I) = T(I)
 12     CONTINUE
        A0 = A0/M0
        R0 = R0SUM - A0*A0*M0
        A(1) = (A(1)/M(1))*10.0**(-IEXP)
        R(1) = R0 - A(1)*A(1)*M(1)*10.0**IEXP
        DO 13 I = 2,ITL
        A(I) = (10.0**(-(I-3)*IEXP))*A(I)/(M(I)*10.0**(3*IEXP))
 13     R(I) = R(I-1)-10.0**((I-3)*IEXP)*A(I)*A(I)*M(I)*10.0**(3*IEXP)
        PRINT 302, A0, (A(I),I = 1,ITL)
        PRINT 303, R0,(R(I),I = 1,ITL)
        DO 15 I = 1,ICT
        Y = A0
        YM = Y
        DO 14 J = 1,ITL
        Y = Y + A(J)*TS(I,J)
 14     YM = YM +((-1)**J)*A(J)*TS(I,J)
        IP = I + IMAX
        IM = IMAX + 2 - I
        RN(IP) = Y
 15     RN(IM) = YM
        RETURN
        END
-AN  XQT  TCH
```